Journal of Medicinal Chemistry



Article

# Discovery and Optimization of Small Molecules Targeting the Protein-Protein Interaction of Heat Shock Protein 90 (Hsp90) and Cell Division Cycle 37 (Cdc37) As Orally Active Inhibitors for the treatment of colorectal cancer

Lei Wang, Jingsheng Jiang, Lixiao Zhang, qiuyue zhang, Jianrui Zhou, Li Li, Xiao-Li Xu, and Qi-Dong You

*J. Med. Chem.*, **Just Accepted Manuscript** • DOI: 10.1021/acs.jmedchem.9b01659 • Publication Date (Web): 14 Jan 2020



## Just Accepted



is published by the American Chemical Society. 1155 Sixteenth Street N.W., Washington, DC 20036

# Discovery and Optimization of Small Molecules Targeting the Protein-Protein Interaction of Heat Shock Protein 90 (Hsp90) and Cell Division Cycle 37 (Cdc37) As Orally Active Inhibitors for the Treatment of Colorectal Cancer

Lei Wang [1,2], Jingsheng Jiang [1,2], Lixiao Zhang [1,2], Qiuyue Zhang [1,2], Jianrui Zhou [1,2], Li Li [1,2], Xiaoli Xu [1,2,*], Qidong You [1,2,*]

[1]State Key Laboratory of Natural Medicines and Jiang Su Key Laboratory of Drug Design and Optimization, China Pharmaceutical University, Nanjing 210009, China.
[2]Department of Medicinal Chemistry, School of Pharmacy, China Pharmaceutical University, Nanjing 210009, China.

*To whom correspondence should be addressed:
Xiaoli Xu, Ph.D.
Phone: +86-15261483858
E-mail: xuxiao_li@126.com

Prof. Qidong You, Ph.D.
Phone: +86 025 83271351
E-mail: youqd@163.com

**Abstract**

Cdc37 is known to work as a kinase-specific cochaperone, which selectively regulates the maturation of kinases through protein-protein interaction (PPI) with Hsp90. Directly disrupting the Hsp90-Cdc37 PPI is emerging as an alternative strategy to develop anticancer agents through a specific inhibition manner of kinase clients of Hsp90. Based on a first specific small molecule inhibitor targeting Hsp90-Cdc37 PPI (**DDO-5936**), which was previously reported by our group, we conducted a preliminary investigation of the structure-activity relationships and pharmacodynamic evaluations to improve the potency and drug-like properties. Here, our efforts resulted in a currently best inhibitor **18h** with improved binding affinity ($K_d$ = 0.5 μM) and cellular inhibitory activity ($IC_{50}$ = 1.73 μM). Both *in vitro* and *in vivo* assays revealed **18h** could efficiently block the Hsp90-Cdc37 interaction to specifically inhibit kinase clients of Hsp90. Furthermore, **18h** showed ideal physiochemical properties with favorable stability, leading to an oral efficacy *in vivo*.

## Introduction

Molecular chaperone heat shock protein 90 (Hsp90) is one of the most abundant intracellular protein, which plays a significant role for its client proteins in correct folding, maturation and stability[1-3]. A considerable number of client proteins of Hsp90 are fundamental effectors in the growth and proliferation of cancer cells[4]. In the past decade, directly targeting the Hsp90 ATPase pocket was considered as a promising anti-cancer target[5-7]. Although several small molecule inhibitors have entered into clinical trials, inevitable heat shock response, limited efficacy and diverse toxicities become the formidable obstacles for them to be approved to the market[8-9]. Apparently, directly inhibiting the activity of Hsp90 ATPase totally blocked the ATP hydrolysis, leading to a nonselective degradation of all the clients of Hsp90 as well as a feedback of heat shock response (HSR)[1, 10]. In fact, during the chaperone cycle, Hsp90 works with the help of many co-cochaperones through diverse protein-protein interactions (PPIs)[11-12]. Different co-chaperones exhibit disparate functions and play specific roles in the dynamic cycle[5, 13]. Among them, cell division cycle 37 (Cdc37) is responsible for selectively recognizing and recruiting the kinase clients, revealing direct and high correlations with diverse cancers[12]. In the Hsp90-Cdc37-kinase recruitment cycle, Cdc37 selectively recognizes the C lobe of unfolded kinase clients (eg. CDK4) under a phosphorylated condition by CK2[14]. Then, the complex of Cdc37-CDK4 binds to an open state of Hsp90. At this stage, Cdc37 interacts with Hsp90 N-terminus via its M domain, as shown in the co-crystal structure (PDB: 1US7)[15]. Subsequently, Cdc37-CDK4 complex shifts to Hsp90 M domain before ATP is captured by Hsp90, making Hsp90 turns to a closed state (PDB: 5FWL). Finally, the captured ATP is fully hydrolyzed and Hsp90 opens to provide a chance for correct folding of CDK4, after which all the components release with the help of PP5 to de-phosphorylate p-Cdc37 (Figure 1)[16]. Thus, a dynamic recruitment cycle of Hsp90-Cdc37-kinases reminds us that inhibition of ATP hydrolyzation is only a rate-limiting step of Hsp90. Different with directly inhibiting ATPase, targeting Hsp90-Cdc37 PPI reveals as an alternative strategy to block the maturation of kinases

to achieve cancer therapy with specificity and safety[17]. In addition, elevated levels of Cdc37 were observed in proliferating cancer cells while normal tissues required little Cdc37, which provided a potential therapeutic window[18]. Recently, many structural studies combined with computational methods of Hsp90-Cdc37-kinase interaction were reported, indicating a more rational way to understand the recognition mechanism[19]. Using NMR and computational studies, the structure-based network of protein kinase clients to the Hsp90-Cdc37 chaperone is emerging and allosteric regulation manner is becoming feasible[20-21]. Structural characterization of Hsp90-Cdc37 also provide important evidence including critical interactions and binding sites[22].

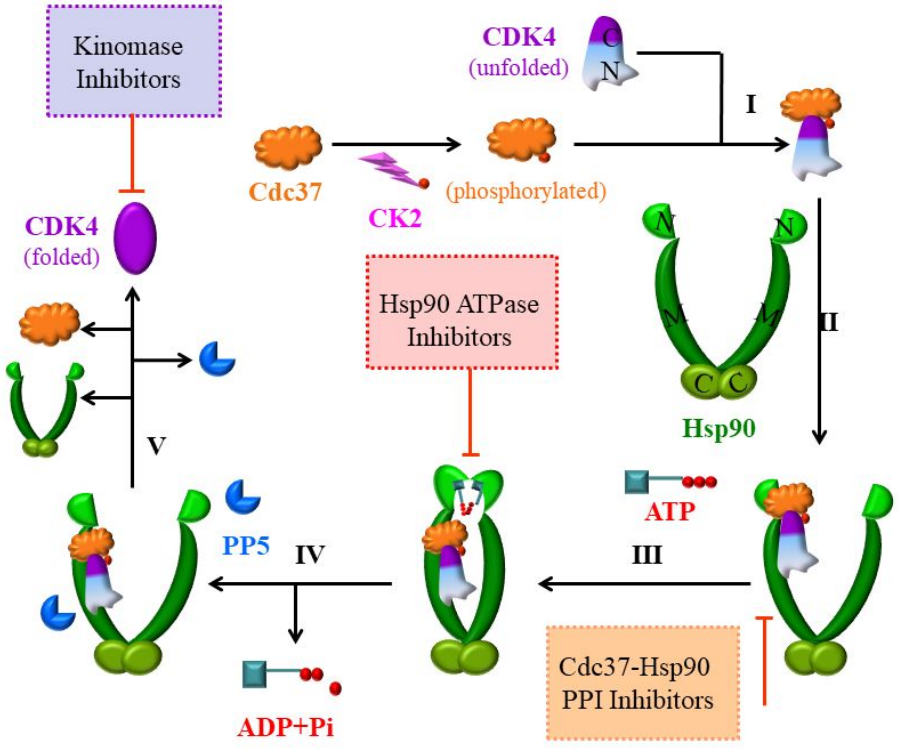


**Figure 1. Hsp90-Cdc37 chaperone cycle for kinase recruitment.** (Ⅰ) With the help of Casein kinase 2 (CK2), Cdc37 is phosphorylated to bind the C lobe of the unfolded kinase client (such as CDK4). (Ⅱ) The complex of Cdc37-kinase subsequently binds to the open state of Hsp90. At this time, M domain of Cdc37 interacts with the N-terminus of Hsp90 (PDB: 1US7). (Ⅲ) Hsp90 captures ATP and turns to a closed state, resulting in Cdc37-kinase complex transferred to M domain of

Hsp90 (PDB: 5FWL). (Ⅳ) When ATP is hydrolyzed, N terminus of Hsp90 opens to provide a chance for kinase folding in a Cdc37-kinase bound state. (Ⅴ) After kinase is totally folded, PP5 helps the de-phosphorylated process of Cdc37. Finally, kinases and Cdc37 are displaced and released.

Currently, small molecular inhibitors with the ability to directly target Hsp90-Cdc37 PPI are rarely reported. At the very beginning, several natural products with anti-cancer potency were found to disrupt Hsp90-Cdc37 PPI in cells by co-IP assays. Although most of them were identified with multiple intracellular targets, they were the first evidence to demonstrate the feasibility of targeting Hsp90-Cdc37 PPI to achieve potential cancer therapy (Figure 2). Among them, **celastrol** (extract of *celastranceae* plants) was one of the most studied natural products for its explicit anti-cancer potency[23-24]. However, the direct binding site of **celastrol** to disrupt Hsp90-Cdc37 PPI remains controversial, including Hsp90 C-terminus (determined by fingerprinting assay) and Hsp90 N-terminus (predicted by molecular docking)[25]. Another more convincing result illustrated that **celastrol** covalently bound to Cdc37, leading to vanishing peaks in NMR assay determined by HSQC spectrum[26]. **Withaferin A** (**WA**), a bioactive compound from extract of *Withania somnifera*, and **FW-04-804**, an extract from the culture broth of soil *Streptomyces*, were also reported to reveal their anti-proliferative activity through a mechanism involving Hsp90-Cdc37 PPI inhibition[27-28]. In addition, **Kongensin A** (**KA**), a natural product isolated from *Croton kongensis*, was reported to covalently bind to a previously undiscovered site involving cysteine 420 in the middle domain of Hsp90, resulting in dissociation of Hsp90 from Cdc37 and providing an original site for the design of covalent inhibitors[29]. Different with the above natural products, **VS-8** was a non-natural compound targeting Hsp90-Cdc37 PPI discovered by our group through virtual screening based on the peptides of Hsp90-Cdc37 binding interface. Although **VS-8** could bind to Hsp90 with a moderate $K_D$ value of 80.4 μM, its accurate binding site remained unclear and the inhibitory function of Hsp90-Cdc37 PPI in cells was

unkonwn[30]. In 2018, another small molecular inhibitor (**DCZ3112**) was reported to exert anti-tumor activity against HER-2 positive breast cancer through inhibition of Hsp90-Cdc37 PPI with a $K_d$ value of 4.98 μM. In fact, although the direct binding site of DCZ3112 was unclear, it provided important clues for potential therapeutic effects by pharmacologically targeting Hsp90-Cdc37 PPI[31].

Recently, our group reported that specifically disrupting the Hsp90-Cdc37 PPI with small molecules was feasible to achieve potential therapeutic effects for colorectal cancer by selectively down-regulating the kinase clients of Hsp90 and arresting the cell cycle without heat shock response[32]. Based on the discovery of hit **compound 11**(Figure 2), we identified **DDO-5936** as a novel Hsp90-Cdc37 PPI inhibitor with potency and specificity through binding to a critical site on Hsp90 involving Glu47 (the most important binding determinants for Hsp90-Cdc37 PPI discovered by our group). Here, on the basis of our previous work, we reported the structure-activity (SAR) and structure-property (SPR) relationships of **compound 11** and **DDO-5936**. The optimized compound **18h** showed ~10 folds enhancement of binding affinity ($K_d$ = 0.5 μM) and cellular inhibitory activity against HCT116 cells ($IC_{50}$ = 1.73 μM). Physicochemical properties were also improved, especially the cell membrane permeability, which resulted in enhanced activities in cells. Both *in vitro* and *in vivo* assays confirmed that **18h** efficiently disrupted Hsp90-Cdc37 PPI, selectively down-regulated kinase clients of Hsp90 and arrested cell cycle in phase $G_0/G_1$ to achieve anti-proliferation effects. Notably, compared with **DDO-5936**, **18h** exhibited much better stability in plasma and liver microsome, leading to favorable anti-cancer effects in the HCT116 tumor xenograft model by oral administration, while **DDO-5936** showed limited oral efficiency. These results suggested that Hsp90-Cdc37 PPI inhibitors can achieve potential anti-cancer therapeutic effects with preferable selectivity and safety, providing a novel insight for the design of inhibitors by targeting molecular chaperone pathways. **18h** represented as a class of promising inhibitors targeting Hsp90-Cdc37 PPI.

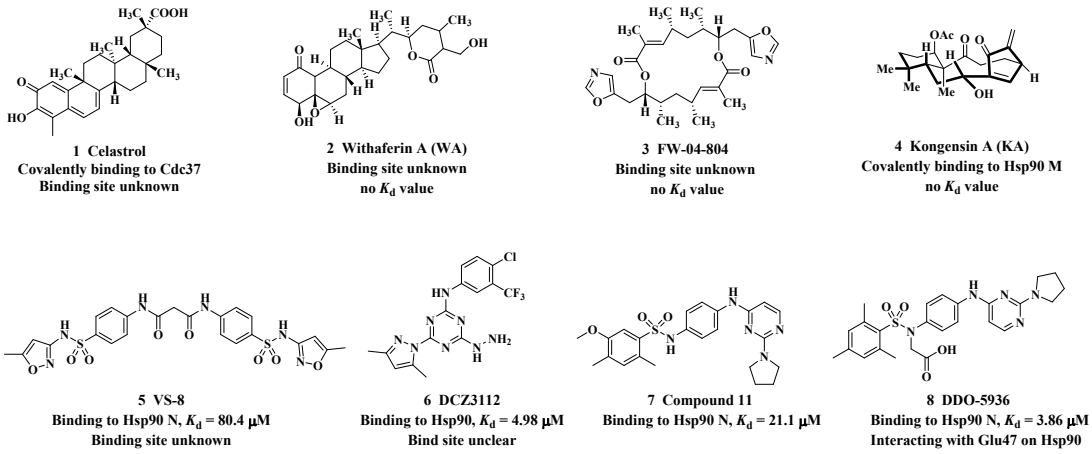


**Figure 2. Previously reported natural products involving a Hsp90-Cdc37 PPI inhibition mechanism and small molecule inhibitors targeting Hsp90-Cdc37 PPI.**

## Results and Discussion

***Preliminary SAR Study Revealed DDO-5936 with Potent Activity.*** On the basis of the discovery of **7** (**compound 11**, chemical structure shown in Figure 3A), which exhibited moderate potency to disrupt Hsp90-Cdc37 PPI ($K_D$ = 21.1 μM, inhibition rate ~56% at 100 μM), our efforts were firstly focused on the improvement of the binding affinity and physical chemical properties. Although **7** emerged as a potential start compound, its binding affinity could not be determined by ITC or NMR assays, which might due to its poor solubility and low activity. Based on the previous results and guided by the potential binding mode of **7** (Figure 3B), we conducted a most important hydrogen bond formed between Glu47 of Hsp90 and imino group of **7**. Then, we split the chemical structure of **7** into three parts, including A ring substituents (which is surrounded by hydrophobic residues involving Phe213), sulfamide part (exhibiting potential space reaching to both protein surface and solvent) and pyrimidine substituents (close to a polar pocket involving Ser50, Asn51, Ser53 and Asp54), shown in Figure 3A. As shown in Table 1, A ring of **7** was replaced with diverse substituted benzene (Scheme 1). Among all the derivatives, compound **12c** (2,4,6-trimethy phenyl substituted) exhibited potent inhibitory ability with 66.0% inhibition rate, leading to an ideal activity at current stage. However, the

inhibition rate of the compounds with mono-substituted benzene were dramatically decreased to below 20%, including **12a** (4-trifluoromethyl phenyl substituted), **12d** (4-methoxyphenyl substituted) and **12e** (4-tertbutyl phenyl substituted). Compounds with di-substituted benzene were not ideal either, both **12f** (2,4-dimethoxyphenyl substituted) and **12g** (2,5-dimethoxyphenyl substituted) showing low inhibition rates in HTRF assay. In addition, compound **12b** demonstrated that larger occupation with naphthalene was not suitable for this site either. Thus, **12c** was the most suitable group for A ring optimization for its favorable inhibitory activity.

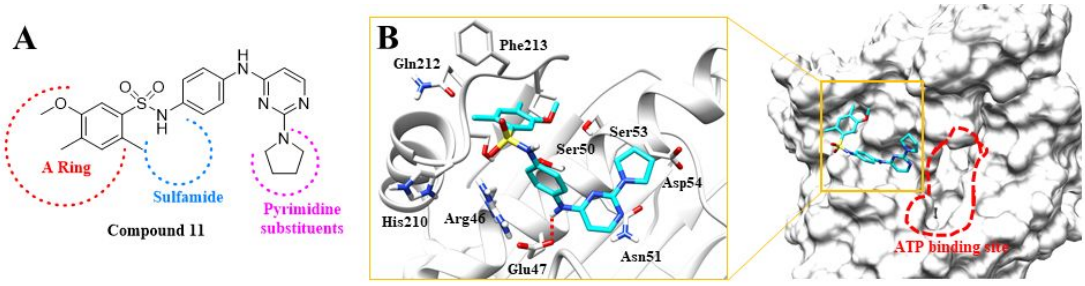


**Figure 3. Binding mode of compound 11 and the optimization strategies.** (A) Chemical structure of **compound 11** and the three sites to be optimized according to the binding mode. (B) **Compound 11** binds to a surface site next to the Hsp90 ATPase pocket (PDB code 2K5B), interacting with the critical residues (forming hydrogen bond) of Hsp90 including Glu47 (binding determinant for Hsp90-Cdc37 PPI). ATPase site on Hsp90 is enclosed and highlighted. Hsp90 is shown in white ribbon and the **compound 11** is shown as cyan stick, respectively. Hydrogen bonds are indicated with red dashed lines.

**Table. 1 Structure-Activity Relationships of different substitution on A ring.**

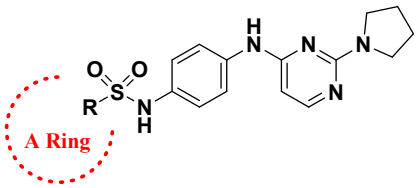


| Comp· | R | Inhibition rate (%)[a] | Comp. | R | Inhibition rate (%)[a] |
|---|---|---|---|---|---|

| | | | | | |
|---|---|---|---|---|---|
| **Comp.11** | 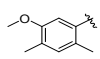 | 56.3 ± 9.4 | **12d** |  | **<** 20 |
| **12a** |  | **<** 20 | **12e** |  | **<** 20 |
| **12b** |  | 46.7 ± 5.2 | **12f** |  | 36.2 ± 4.9 |
| **12c** |  | 66.0 ± 8.7 | **12g** |  | 41.8 ± 5.0 |

[a] All inhibition rates were determined using 100 μM compound.

Considering the tri-methyl phenyl was important for activity, we further tried to investigate the substituents on sulfamide with tri-methyl phenyl remaining on A ring. Based on the chemical structure of **12c**, multiple side chains were employed to obtain **15b** (previously reported as **DDO-5936**) with improved activity. As shown in Table 2, benzyl groups were not appropriate in reducing the inhibition rates below 50%, including **15d** (4-benzoic acid substituent), **15e** (4-isopropyl phenyl substituent), **15f** (4-chloro phenyl substituent) and **15g** (4-methoxy phenyl substituent). Both **15a** and **15b** showed ideal inhibition rates of 65.4% and 72.6% respectively, indicating a tolerable modification by employing a side chain of acetic acid. Although **15b** only slightly improved the *in vitro* activity, including a 72.6% inhibition rate by HTRF assay and a moderate binding affinity by BLI ($K_D$ = 7.41 μM), it could be detected by ITC ($K_d$ = 7.81 μM, Figure S2) and NMR assays (previously determined by CPMG, STD and HSQC) [32], which illustrated an explicit binding affinity and a pivotal binding site to disrupt Hsp90-Cdc37 PPI (Table 4). **15b** exhibited anti-proliferative potency with an $IC_{50}$ value of 10.24 μM against HCT116 cells (Cdc37 high expression), a lower activity with an $IC_{50}$ value of 55.74 μM against A549 cells (Cdc37 low expression) and almost no activity against normal hepatocyte (L02). Although **15b** exhibited as an initial compound with moderate potency, it was still urgent to enhance its binding affinity and *in vivo* efficiency. In addition, **15b** showed non-ideal stability in plasma or liver microsome (Table 6 & Table 7), as well as an oral inefficacy in *in vivo* models. Thus, our next task was to optimize its binding

affinity, anti-proliferation activity, stability and physicochemical properties to achieve a more potent Hsp90-Cdc37 PPI inhibitor both *in vitro* and *in vivo*.

**Table.2 Structure-Activity Relationships of Different Substituents on Sulfamide.**

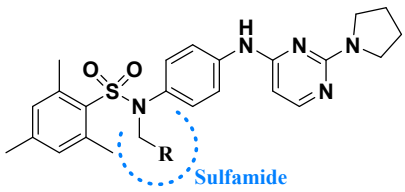


| Comp. | R | Inhibition rate (%)[a] | Comp. | R | Inhibition rate (%)[a] |
|---|---|---|---|---|---|
| **12c** | - | 66.0 ± 10.1 | **15d** | 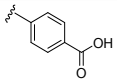 | 52.8 ± 4.8 |
| **15a** |  | 65.4 ± 7.4 | **15e** |  | < 50 |
| **15b (DDO-5936)** |  | 72.6 ± 3.5 | **15f** |  | < 50 |
| **15c** |  | < 50 | **15g** | 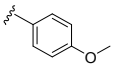 | < 50 |

[a] All inhibition rates were determined using 100 μM compound.

***Further SARs Led to 18h with Improved Binding Affinity and Anti-proliferation Activity.*** On the basis of **15b**, we further investigated the pyrimidine substituents to explore the pocket with the aim to improve activity on this site. As shown in Table 3, we firstly replaced the pyrrolidine group with methylamine and ethylamine, resulting in compound **17a**, **18a** and **17b**, **18b** with dramatic activity loss (less than 50%). Similarly, substituents including cyclopropylamine (compound **17c** and **18c**) and pentan-3-amine (compound **17d** and **18d**) exhibited low inhibition rates (Table 3), indicating an unfavorable flexibility site on this region. Interestingly, **17e** with diethylamine substituent exhibited low activity while **18e** showed a considerable inhibition rate of 79.58%. Understanding the region of pyrimidine-substituents was not suitable for the flexible chains, we next employed piperidine and azepane with

larger rings, to compare with pyrrolidine-substituted **DDO-5936**. Notably, **17f** and **18f** maintained inhibitory activity with inhibition rates of 79.11% and 86.17%, respectively. However, **17g** and **18g** reduced the inhibitory activity to below 50%, demonstrating an unfavorable employment of larger groups. Encouraged by **17f** and **18f**, we subsequently employed more polar groups including piperazine and *N*-methyl piperazine to obtain compound **17h**, **18h** and **17i**, **18i**. Although **17i** and **18i** maintained activity, **17h** and **18h** exhibited best inhibition rates (95.48% and 97.41%, respectively) which were worthy of further evaluation.

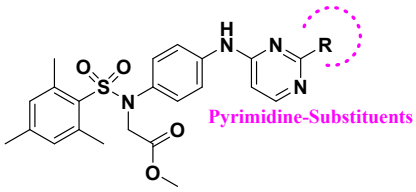


**17 a-i**

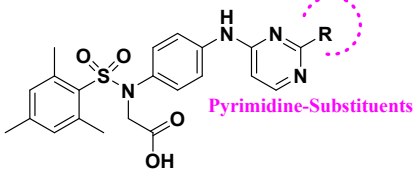


**18 a-i**

**Table. 3 Structure-Activity Relationship of Pyrimidine-Substituted compounds.**

| R | Comp. | Inhibition rate (%)[a] | Comp. | Inhibition rate (%)[a] |
|---|---|---|---|---|
|  | **17a** | < 50 | **18a** | < 50 |
|  | **17b** | < 50 | **18b** | < 50 |
|  | **17c** | < 50 | **18c** | < 50 |
|  | **17d** | < 50 | **18d** | < 50 |
|  | **17e** | < 50 | **18e** | 79.58 ± 4.1 |
|  | **17f** | 79.11 ± 3.3 | **18f** | 86.17 ± 6.0 |
|  | **17g** | < 50 | **18g** | < 50 |
|  | **17h** | 95.48 ± 5.7 | **18h** | 97.41 ± 6.2 |
|  | **17i** | 70.13 ± 2.9 | **18i** | 71.09 ± 4.8 |

[a] All inhibition rates were determined using 100 μM compound.

Considering the results that different side chains of **17h** and **18h** (methyl acetate and acetic acid respectively) showed similar inhibitory activity, we next explored more substituents and bioisosteres of acetic acid of **18h**. As shown in Table 4, inhibitors including **17h**, **18h**, **19** and **21** all showed parallel inhibitory activities (inhibition rates exceeded 95%), while **20** exhibited an activity loss to only 64.31%. We subsequently conducted thermal shift assay to determine the potential binding affinity, leading to **17h** and **18h** with maximum $\Delta T_m$ values of 3.53 and 4.75 $^oC$, respectively, which showed superior results compared with 2.13 $^oC$ of **DDO-5936**. In order to comprehensively investigate the binding processes and kinetic profiles, binding assays including both BLI (binding kinetics) and ITC (binding thermodynamics) were carried out to determine the precise binding affinities. Consistent with thermal shift assay, **17h** and **18h** exhibited the most potent binding affinity to Hsp90, leading to an improved *in vitro* activity comparing to **DDO-5936**. Especially for **18h**, which could be regarded as a first compound with binding affinity below one micromolar ($K_D$ = 0.50 μM by BLI assay and $K_d$ = 0.63 μM by ITC assay, Figure 4A and 4B).Although $K_{on}$ value of **18h** slightly decreased to 10600 $Ms^{-1}$ (compared to **DDO-5936**, $K_{on}$ = 16800 $Ms^{-1}$), a comparably low dissociation rate was observed than other compounds ($K_{off}$ = 0.005 $s^{-1}$), which contributed most to the increased binding affinity. In ITC assay, both entropy change ($-T\Delta S$ = -4.52 kcal/mol) and enthalpy change ($\Delta H$ = -3.96 kcal/mol) favorably contributed to gibbs free energy of **18h**. Unfortunately, **17h**, **19** and **20** all showed similar binding affinity with **DDO-5936** in thermal shift assay, BLI assay and ITC assay (Table 4). In addition, $\Delta G$ values from the computational tools (MM-GBSA) also showed consistent results with ITC experiments (Table S2).

Consistent results were observed in the T1ρ NMR spectra assays (Figure S3), indicating that the WT Hsp90 protein significantly interfered with **18h**. Meanwhile, three mutants (R46A, E47A and Q133A) exhibited less effects on **18h**, especially mutant E47A, showing a little effect on CPMG spectrum of **18h** which demonstrated

that Glu47 of Hsp90 was one of the binding determinants for **18h**. In addition, positive saturation transfer difference (STD) spectra was also employed to detect STD signals, which reconfirmed that **18h** directly bound to Hsp90 (Figure 4C). We further compared the potential binding modes between **18h** and **DDO-5936**. As shown in Figure 5, **18h** occupied a similar binding site of **DDO-5936**, a cleft next to the ATPase pocket, forming a critical hydrogen bond with Glu47 on Hsp90. Piperazine substituent might exhibit a better adaption to the pocket involving Ser50, Asn51 and Asp54. In addition, all the compounds including **17h**, **18h**, **19**, **20**, **21** and **DDO-5936** exhibited no inhibition on Hsp90 ATPase activity ($IC_{50}$ **>** 100 μM), using AT13387, a phase Ⅱ Hsp90 inhibitor targeting ATPase site, as reference ($IC_{50}$ = 150 nM, Table S1). Together, all the results demonstrated an explicit binding mechanism of **18h** with a ~10 folds improvement on *in vitro* binding affinity comparing to **DDO-5936**.

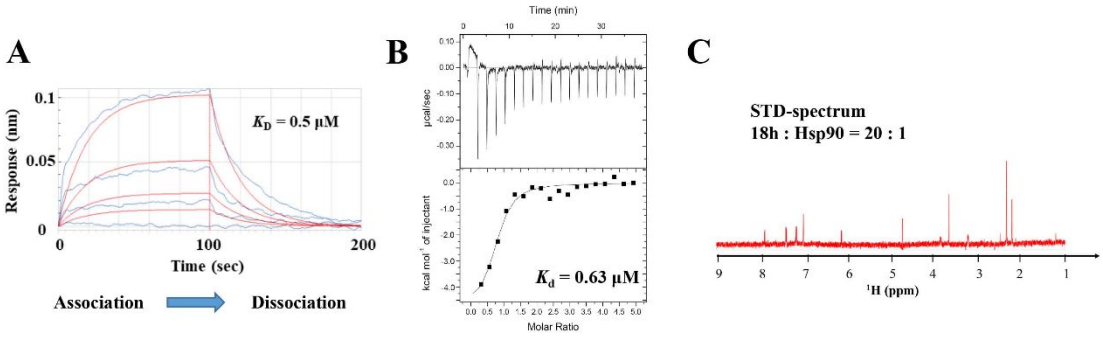


**Figure 4. 18h directly bound to Hsp90.** (A) Binding affinity of **18h** with Hsp90 protein, determined by binding kinetic assay of biolayer interferometry (ForteBio Octet). The $K_D$ value was 0.5 μM. (B) Direct binding experiments of Hsp90 and **18h**, determined by binding thermodynamic assay of ITC. The $K_d$ value was 0.63 μM. (C) $^1$H saturation transfer difference (STD) NMR spectrum of 100 μM **18h** binding to 5 μM Hsp90. ppm, parts per million. All data are representative of three independent experiments.

We next evaluated these Hsp90-Cdc37 PPI inhibitors for their cell growth inhibitory activity against two cancer cell lines including HCT116 (Cdc37 high expression) and A549 (Cdc37 low expression) and a non-cancer cell line (L02,

normal human liver cells). Although all the derivatives showed efficiency in cells (Table 4), **18h** exhibited both the preferable antiproliferative activity against HCT116 cells ($IC_{50}$ = 1.73 μM) and the best selectivity ($IC_{50}$ **>** 50 μM against A549 and L02).

**Table 4. Determination of in vitro inhibition activity and binding affinities of Hsp90-Cdc37 PPI inhibitors using HTRF, thermal shift, BLI, ITC and antiproliferative activities by CCK8 assay.**

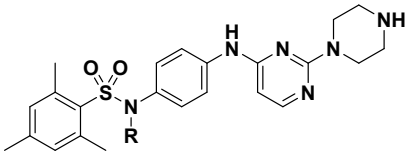

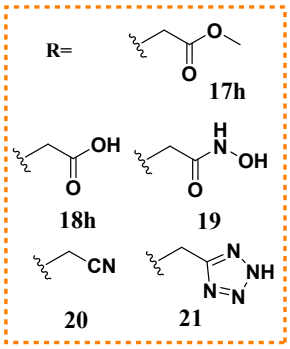


| Comp. | Inhibition rate (%)[a] | $\Delta T_m$ (℃) [b] | Binding Kinetics (BLI) [b] | | | Binding Thermo Dynamics (ITC) [b] | | | Antiproliferative activities $IC_{50}$ (μM) | | |
|---|---|---|---|---|---|---|---|---|---|---|---|
| | | | $K_D$ (μM) | $K_{on}$ ($Ms^{-1}$) | $K_{off}$ ($s^{-1}$) | $K_d$ (μM) | ΔH (kcal/mol) | -TΔS (kcal/mol) | HCT116 | A549 | L02 |
| **17h** | 95.48 ± 4.7 | + 3.53 | 1.97 | 20300 | 0.04 | 1.73 | -1.96 | -5.90 | 6.25 ± 1.2 | 43.26 ± 8.9 | > 50 |
| **18h** | 97.41 ± 6.2 | + 4.75 | 0.50 | 10600 | 0.005 | 0.63 | -3.96 | -4.52 | 1.73 ± 0.6 | > 50 | > 50 |
| **19** | 96.24 ± 4.9 | + 1.59 | 2.66 | 6350 | 0.02 | 5.49 | -0.56 | -6.62 | 3.94 ± 0.8 | 16.23 ± 2.2 | 21.94 ± 2.3 |
| **20** | 64.31 ± 2.3 | + 1.10 | - | | | - | | | - | - | - |
| **21** | 98.58 ± 3.4 | + 1.36 | 5.50 | 7010 | 0.04 | 2.40 | -1.61 | -6.06 | 5.42 ± 1.7 | 37.94 ± 2.7 | > 50 |
| **15b (DDO-5936)** | 72.60 ± 3.5 | + 2.13 | 7.41 | 16800 | 0.13 | 7.81 | -4.17 | -2.80 | 10.24 ± 3.9 | 55.74 ± 9.8 | > 50 |

[a] All inhibition rates were determined using 100 μM compound.

[b] Determined against Hsp90 alone.

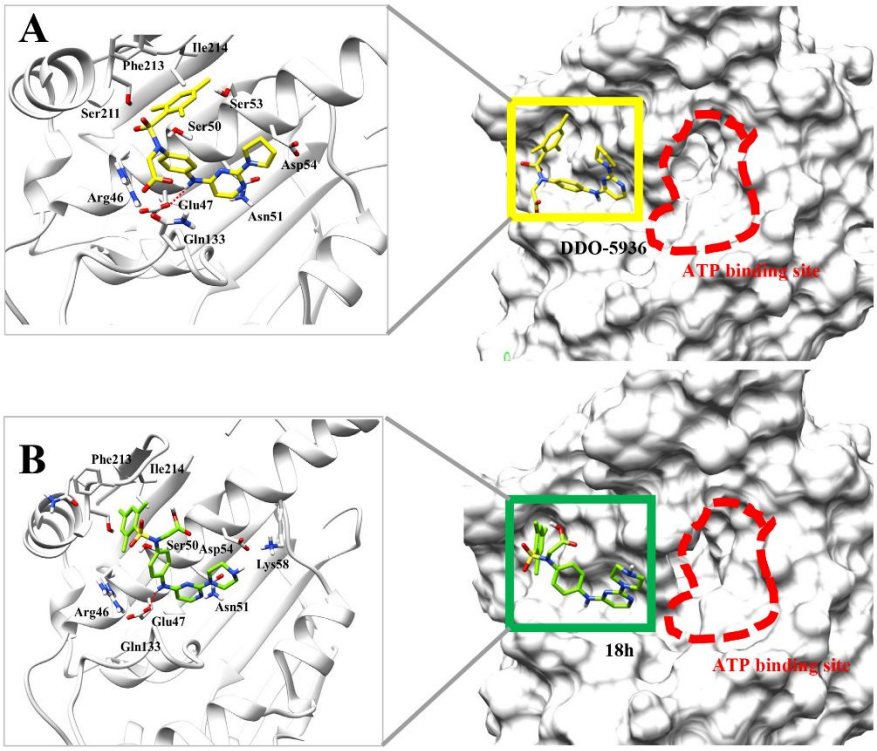


**Figure 5. Predicted binding mode of DDO-5936 and 18h in Hsp90-Cdc37 binding sites (PDB ID: 1US7).** (A) Binding pattern of **DDO-5936** to Hsp90 (PDB code 2K5B). The compound is shown in yellow stick and Hsp90 is shown in white ribbon. (B) Binding pattern of **18h** to Hsp90 (PDB code 2K5B). The compound is shown in green stick and Hsp90 is shown in white ribbon. Hydrogen bonds are shown in red dashed lines and the residues in the binding site are labeled. ATP binding site is circled in red dashed lines and highlighted.

***Physicochemical Properties of 18h and Its Derivatives.*** To evaluate the drug-like properties of **18h** and its derivatives, lipid−water distribution coefficients (ClogP) were computationally calculated through ACD lab and experimentally determined on a Gemini Profiler instrument (pION) by the potentiometric titration method, similar as previously reported[33]. The permeability coefficients (Pe) were determined by a standard parallel artificial membrane permeability assay (PAMPA) on a PAMPA Explore instrument (pION). As shown in Table 5, **18h** displayed improved permeability at pH 7.4, compared with **DDO-5936** and **compound 11**. All the

compounds showed reasonable lipid−water distribution coefficients, while compound **19**, **20**, **21** showed limited or decreased permeability.

**Table 5. Physicochemical Properties of the compounds 17h, 18h, 19, 20, 21 and DDO-5936.**

| Comp. | ClogP | log *D*, pH 7.4 | Pe, pH 7.4 ($10^{-6}$cm/s) |
|---|---|---|---|
| **17h** | 3.98 | 2.63 | 101.22 |
| **18h** | 3.52 | 1.93 | 104.35 |
| **19** | 2.21 | 0.82 | 44.10 |
| **20** | 3.36 | 2.01 | 61.49 |
| **21** | 2.62 | - | 55.37 |
| **15b (DDO-5936)** | 4.54 | 1.67 | 70.42 |
| **Compound 11** | 5.00 | 4.82 | 65.87 |

***18h Showed Preferable Stability in Plasma and Liver Microsomes.*** As **18h** showed ideal physicochemical properties and improved activities on cellular level, we further evaluated the stability of **18h** in mouse and human plasma as well as *in vitro* metabolic stability in human and mouse liver microsomes, using **DDO-5936** as reference. As shown in Table 6, **18h** showed preferable stability both in mouse plasma and human plasma, exhibiting an approximately 100% compound retention after 90 minutes incubation. However, **DDO-5936** showed only 59% remain in mouse plasma and 62% in human plasma after 90 minutes incubation, indicating a feeblish stability which might limit its further *in vivo* efficacy. The *in vitro* metabolic stability of the two compounds was assessed both in human liver microsomes and mouse liver microsomes (Table 7). **18h** possessed better metabolic stability with half-life values of 124.5 minutes in human liver microsomes and 96.3 minutes in mouse liver microsomes, compared with 30.4 minutes and 16.82 minutes of **DDO-5936** respectively. Meanwhile, **18h** also revealed lower clearance rates. Thus, **18h**

exhibited promising stability and was worthy for further development.

**Table 6. Stability of DDO-5936 and 18h in mouse and human plasma.**

| Incubation Time (min) | DDO-5936 remained | | 18h remained | |
|---|---|---|---|---|
| | Mouse Plasma | Human Plasma | Mouse Plasma | Human Plasma |
| 0 | 100% | 100% | 100% | 100% |
| 10 | 100% | 101% | 100% | 98% |
| 30 | 86% | 92% | 102% | 104% |
| 60 | 71% | 76% | 101% | 102% |
| 90 | 59% | 62% | 105% | 103% |

**Table 7. In vitro metabolic stability in human and mouse liver microsomes.**

| Compound | Human liver microsomes | | Mouse liver microsomes | |
|---|---|---|---|---|
| | $T_{1/2}$ (min) | CL (μl/min/mg) | $T_{1/2}$ (min) | CL(μl/min/mg) |
| **DDO-5936** | 30.4 | 32.6 | 16.82 | 59 |
| **18h** | 124.5 | 8.97 | 96.3 | 10.3 |

***MD Simulation Revealed 18h With Favorable Stability.*** In order to explore the binding process and simulate the dynamic course of **DDO-5936** and **18h**, we performed a 50 ns MD simulation based on the binding modes described previously[32]. Based on the simulation trajectory, we extracted five binding modes of each compound at 0, 10, 20, 30, 40 and 50 ns, respectively and conducted them to superimposition modes. As shown in Figure 6, **DDO-5936** started to exhibit an unstable binding mode from 40 ns simulation, exerting an unexpected increase of RMSD values. The binding mode of **DDO-5936** at 50 ns also showed a departure pattern from the binding pocket. In contrast, **18h** showed consistent binding modes from 0 to 50 ns, revealing a preferable stability in this simulation system. Additionally, we calculated the changes of Gibbs free energy of both **DDO-5936** and **18h** at different time point of simulation trajectory (Figure S4). Consistent with other

experimental results, the ΔG values of **DDO-5936** exhibited a markedly decrease at 40 ns simulation (less than -5 kcal/mol remained at 50 ns) while the ΔG values of **18h** showed a constant level during the whole simulation, demonstrating a more stable binding pattern of **18h** compared to **DDO-5936**.

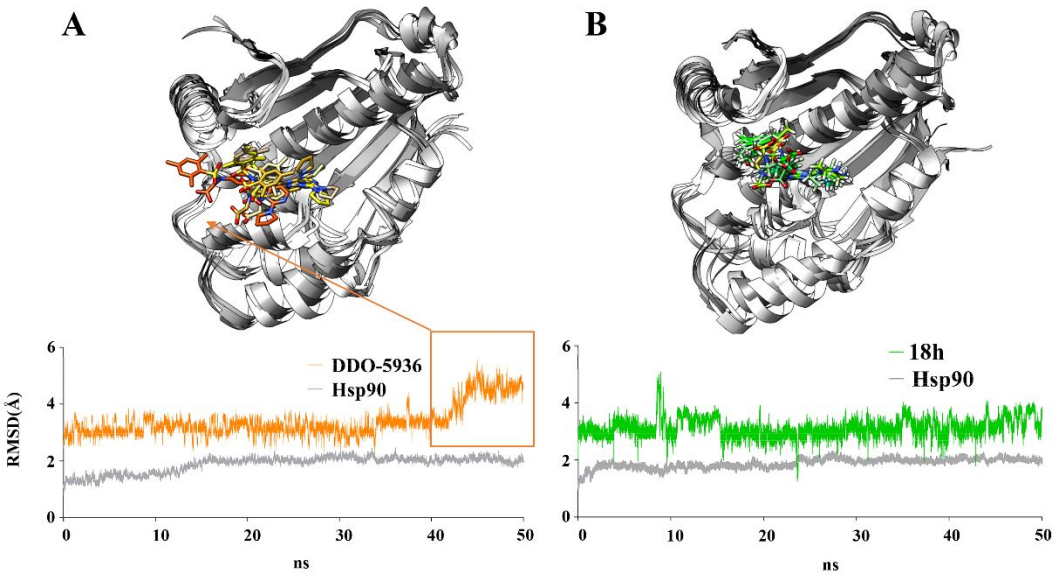


**Figure 6. Molecular dynamic simulation (50ns) revealed 18h with preferable stability.** The superimposition of binding modes of **DDO-5936** (A) and **18h** (B) on 0, 10, 20, 30, 40 and 50 ns. RMSD values of backbone atoms of Hsp90 and the compound were shown to represent the stability. Orange curve represents RMSD values of **DDO-5936** and green curve for **18h**. RMSD values of Hsp90 protein are all displayed with gray curves. Data are representative of three independent experiments.

***18h Efficiently Disrupted Hsp90-Cdc37 PPI in Cells and Selectively Induced Kinase Degradation.*** To confirm the detailed functions and interactions between **18h** and the Hsp90 protein in cells, we further performed a cellular thermal shift assay (CETSA) to demonstrate the binding affinity, cellular uptake and target engagement of **18h** in cells. As shown in Figure 7A, **18h** exhibited ability to thermally stabilize Hsp90 in HCT116 cells by Western blots analysis. Using β-actin as a reference, a detectable phenomenon revealed that Hsp90 showed an explicit distinction between being untreated or treated with 20 μM **18h** for 12 hours, with an alternation of

temperature ranging from 37 to 75 °C, demonstrating a direct binding pattern of **18h** to Hsp90 protein and a preferable cellular uptake. Then, quantitative analysis of these results was calculated to indicate a $T_m$ shift from 51.75 °C to 58.34 °C. $\Delta T_m$ value was + 6.39 °C which showed a consistent result with thermal shift assay ($\Delta T_m$ = + 4.75 °C). Subsequently, we carried out coimmunoprecipitation (co-IP) experiments to determine the Hsp90-Cdc37 PPI inhibition efficacy of **18h** in cells. In order to evaluate the different regulation mechanisms of **18h** compared with Hsp90 ATPase inhibitors, we used AT13387 as a reference. After treatment with **18h** (0, 1, 5, 10 μM) and AT13387 (0, 0.2, 0.5, 1 μM) at different concentrations, respectively, we immunoprecipitated Hsp90 to determine the bait proteins. We distinctly observed that **18h** disrupted the Hsp90-Cdc37 PPI in HCT116 cells with a concentration-dependent manner, while AT13387 showed no inhibition of Hsp90-Cdc37 PPI (Figure 7B). In addition, with Hsp90-Cdc37 being blocked, CDK4 was also detected to be decreased in **18h** treated groups, showing a reasonable and consistent result as previously reported[32]. Thus, both CETSA and co-IP assay indicated **18h** as an efficient small molecule inhibitor targeting Hsp90-Cdc37 PPI in cellular level.

To further identify the specific inhibition effects of **18h** on Hsp90-Cdc37 pathway, we performed Western-blots assays to determine the representative biomarkers of Hsp90-Cdc37 in both concentration-dependent and time-dependent manner. As shown in Figure 7C, **18h** specifically inhibited the kinase clients of Hsp90 (CDK4 and CDK6), leading to downregulation of cyclin D1/cyclin D3 and upregulation of p21/p27. Treatment of **18h** showed no effects on either the glucocorticoid receptor (GR) or its phosphorylated form (p-GR), which was a nonkinase client protein of Hsp90. This result indicated a favorable specificity of selective inhibition of Hsp90 clients as previously reported. Notably, Hsp70 showed no increase after treatment of **18h** to avoid potential heat shock response, which was different with the reactions after treated with Hsp90 ATPase inhibitors. In addition, Hsp90, Cdc37 and p-Cdc37 all showed consistent expression. Therefore, **18h** disrupted Hsp90-Cdc37 PPI through a direct binding mode in cellular lever to achieve a specifically inhibiting manner of

kinase clients of Hsp90.

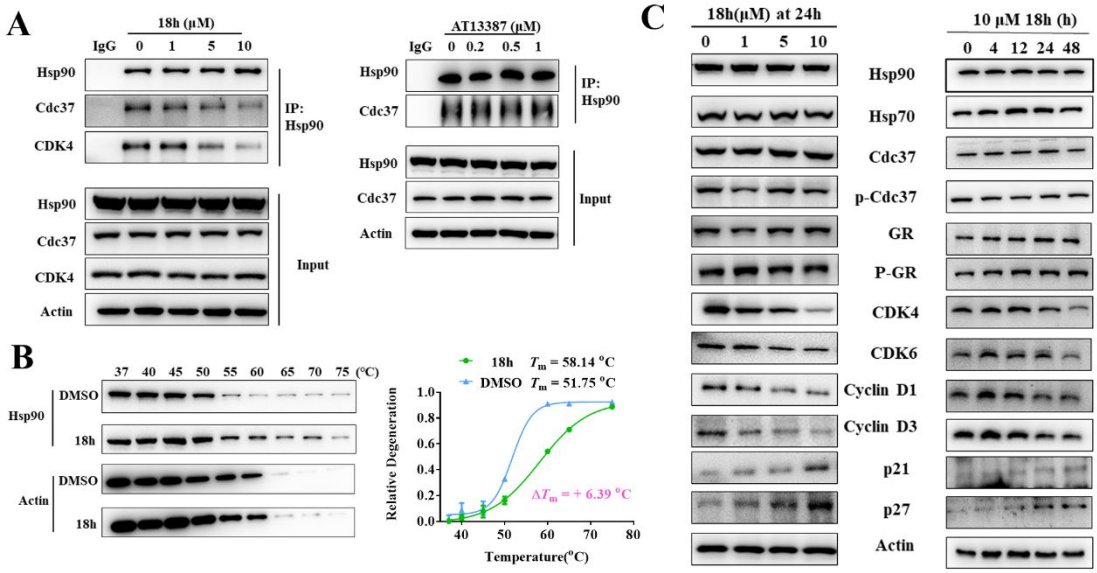


**Figure 7. 18h disrupted the Hsp90-Cdc37 PPI in cells through directly binding to Hsp90, and selectively down-regulated kinase clients of Hsp90 without HSR.** (A) co-IP assay of **18h** (concentrations of the compound increasing from 0, 1, 5 to 10 μM) and AT13387 (0, 0.2, 0.5, 1 μM) in HCT116 cells. **18h** efficiently blocked Hsp90-Cdc37 PPI through a dose-dependent manner, leading to the dissociation of CDK4 from the Hsp90-Cdc37 complex. AT13387 showed no effect on Hsp90-Cdc37 PPI in cells. Western blots were performed with anti-Hsp90, anti-Cdc37, or anti-CDK4 in each experiment. (B) Cellular thermal shift assay of HCT116 cells treated with DMSO or 20 μM of **18h**. β-actin was determined as a loading control. Data are representative of three independent experiments. The gray levels were used to calculate the $T_m$ value of **18h** and DMSO, indicating a $\Delta T_m$ value of + 6.39 °C. (C) Dose-dependent and time-dependent western blot analysis of Hsp90, Hsp70, Cdc37, p–Cdc37, GR, p-GR, CDK4, CDK6, Cyclin D1, Cyclin D3, p21 and p27 protein expression levels in HCT116 cells after treatment with 0, 1, 5 and 10 μM **18h** for 24 hours or treatment with 10 μM **18h** for 0, 4, 12, 24 and 48 hours. β-Actin was used as a loading control. Data are representative of three independent experiments.

***18h Induced Cell Cycle Arrest.*** As previously reported, Hsp90-Cdc37 PPI played a

significant role in the correct folding of CDK4 and exhibited high correlation with cell cycle process and related regulatory effectors[16, 32]. Treatment with **18h** efficiently inhibited CDK4/6 and its downstream effectors (Figure 7C). Based on this result, we subsequently performed a cell cycle distribution analysis following a standard flow cytometry method. HCT116 cells were treated with **18h** (0, 5, 10 μM) for 24 hours or 48 hours, respectively, by staining DNA with propidium iodide (PI). **18h** concentration-dependently and time-dependently enhanced the percentages of HCT116 cells in $G_0$-$G_1$ phase, demonstrating a mechanism of $G_0$-$G_1$ phase arrest to inhibit cell cycle progression (Figure 8).

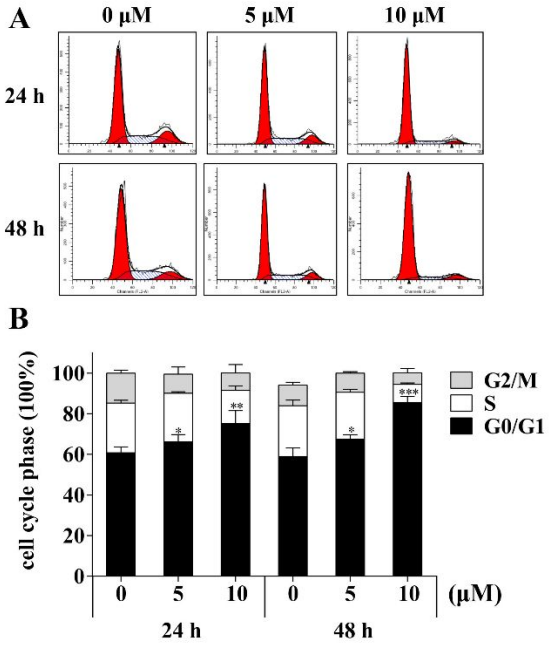


**Figure 8. Cell cycle analysis of compound 18h.** (A) Cell cycle distribution determined by propidium iodide (PI) staining of HCT116 cells after treatment with 0, 5 and 10 μM of **18h** for 24 h or 48 h, respectively. (B) A graphic histogram of cell cycle distribution. All data are representative of three independent experiments as the means ± SD (*$P < 0.05$, **$P < 0.01$, ***$P < 0.001$).

***Pharmacokinetic Profiles of 18h and In Vivo Antitumor Efficacy.*** As shown in Table 8, we determined the pharmacokinetic profiles of **18h** using a single-dose (80

mg/kg, po) in mice bearing HCT116 xenografts tumors. The concentrations of **18h** both in plasma and tumor tissues were measured to indicate favorable properties including the exposure of **18h** (area under the curve) as 533.4 hours·μg/ml in plasma and 132.3 hours·μg/ml in tumor tissue, moderate clearances (186.5 ml/h/kg in plasma and 167.9 ml/h/kg in tumor tissue) and reasonable half-life values ($t_{1/2}$ = 1.46 hours in plasma and 4.66 hours in tumor tissue). Thus, the ideal pharmacokinetic profiles of **18h** led to favorable druglike properties for further efficacy studies *in vivo*.

The *in vivo* antitumor efficacy of **18h** (**DDO-5636** was used for comparison) was evaluated in the same model used in pharmacokinetic assay. In this study, the hydrochloride salt of **18h** and sodium salt of **DDO-5936** were daily treated by intragastric administration at 40 and 80 mg/kg, respectively. As shown in Figure 9A, compound **18h** caused inhibition of tumor growth significantly in a dose-dependent manner. **DDO-5936** exhibited no inhibition effects at low dose (40 mg/kg), indicating an obviously weak potency compared with **18h**, although it showed a moderate effect at high dose group (80 mg/kg). Both **DDO-5936** and **18h** were well tolerated for the absence of serious weight loss during the whole assay (Figure 9B). The results of the *in vivo* antitumor efficacy revealed consistence with previous data. Hematoxylin-eosin (H&E) staining of **18h**-treated and **DDO-5936** high dose groups showed that tumor cells in the xenografts decreased significantly, while **DDO-5936** low dose group exhibited similar results of control group with no inhibition effect (Figure 9C). We also observed a significant decrease of CDK4 in **18h**-treated and **DDO-5936** high dose groups by immunohistochemical staining, while **DDO-5936** low dose group remained no inhibition of CDK4. In addition, both **DDO-5936** and **18h** exhibited little influence on different organs of mice (Figure S4). Thus, these results demonstrated that **18h** showed improved oral availability, compared with **DDO-5936**, to suppress HCT116 xenografted tumor growth *in vivo*.

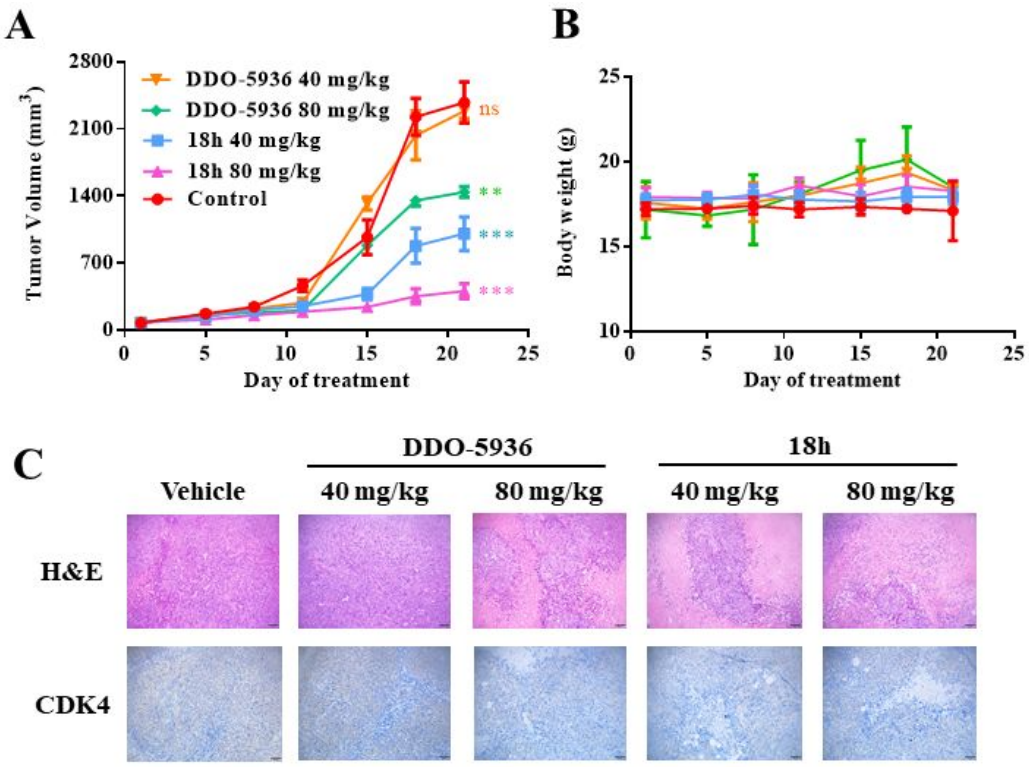


**Figure 9. 18h inhibited xenograft tumor growth in immunocompromised mice.** (A) *In vivo* antitumor efficacy of **DDO-5936** and **18h** in HCT116 xenograft model. Mice were administered **DDO-5936** and **18h** daily (0, 40, 80 mg/kg, respectively) by gavage starting 7 days after cell implantation. Tumor volumes were determined by calipers. The tumor volumes are plotted as the mean ± s.e.m. ($^{*}P$<0.05; $^{**}$ $P$ <0.01; $^{***}$ $P$ <0.001, n = 6). (B) The effects on body weight changes of the mice treated with **DDO-5936** and **18h**. (C) H&E staining showed the tumor tissue morphology of different groups with **DDO-5936** and **18h**. Scale bars were represented as 50 μm. The expression levels of CDK4 were analyzed in tumor tissues by immunohistochemistry.

**Table. 8 Pharmacokinetic profiles of 18h.**

| **Parameters** | **18h** | |
|---|---|---|
| | Plasma | Tumor |
| **$T_{max}$ (h)** | 0.5 | 1 |
| **$t_{1/2}$ (h)** | 1.46 | 4.66 |
| **$C_{max}$(μg/ml)** | 307.5 | 50.0 |

| | | |
|---|---|---|
| **$AUC_{0-t}$(h*μg/ml)** | 533.4 | 132.3 |
| **$AUC_{0-\infty}$(h*μg/ml)** | 536.2 | 167.9 |
| **Vz_F(ml/kg)** | 391.6 | - |
| **Cl_F(ml/h/kg)** | 186.5 | 595.7 |
| **MRT (h)** | 1.46 | 6.02 |

## CONCLUSIONS

Although Hsp90 ATPase inhibitors have been considered effective in anti-cancer treatment, such side effects as inevitable heat shock response, limited efficacy and diverse toxicities are unavoidable, which limit their clinical usage. In the Hsp90 chaperone cycle, the specific functions are achieved by diverse protein-protein interactions with co-chaperones. Cdc37 has been regarded as a kinase-specific co-chaperone with important roles for both Hsp90 and kinases. Different with directly inhibiting ATPase, targeting Hsp90-Cdc37 PPI reveals as an alternative strategy to block the maturation of kinases to achieve cancer therapy with specificity and safety. Development of small molecules targeting Hsp90-Cdc37 PPI shows promising opportunities to understand the Hsp90-Cdc37 chaperone cycle for kinase recruitment. Considering the totally different regulation mechanism, these modulators might be used in combination with other kinase inhibitors to explore more potential utility. In this study, the integration of medicinal chemistry and multiple biochemical tests along with computational methods was used to develop more potent Hsp90-Cdc37 PPI inhibitors (Figure 10). Based on an identified binding mode of **compound 11**, the structure-activity and structure-property relationships of Hsp90-Cdc37 PPI inhibitors were explored to obtain a series of compound exhibiting Hsp90-Cdc37 inhibition potency, resulting in lead compound **18h** with best *in vitro* binding affinity, improved anti-proliferative activity, preferable stability in plasma and microsome, as well as oral efficacy *in vivo*, compared with our previously reported compound **DDO-5936**. In this section, MD simulation and docking models were also employed to guide and explain the results of the compounds. The results of both *in vitro* and *in vivo* assays

confirmed that compound **18h** could efficiently block the Hsp90-Cdc37 PPI through a direct binding mode, leading to a specific down-regulation of kinase clients of Hsp90 and cell cycle arrest to achieve potent anti-proliferative activities. In HCT116 xenografts, **18h** showed promising tumor growth inhibition with no weight loss by oral administration. In summary, **18h** could be regarded as an orally active Hsp90-Cdc37 PPI inhibitor and a promising candidate agent for the treatment of cancer through an alternative way to regulate the function of the molecular chaperone.

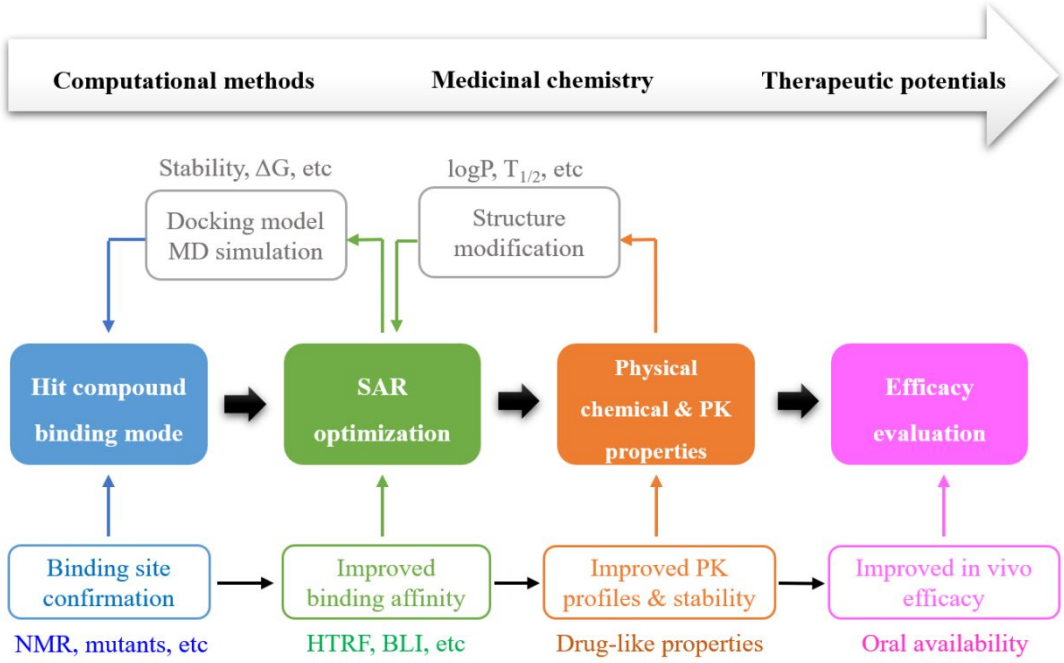


**Figure 10. Schematic overview of the workflow, including the combination of computational methods, medicinal chemistry and therapeutic efficacy evaluation.**

## EXPERIMENTAL SECTION

**General Information.** Unless otherwise mentioned, all of the commercial reagents were directly used without further purification. All the organic solutions were concentrated using an evaporator (BüchiRotavapor) below 60 °C under reduced pressure. All the reactions were visualized using UV light and monitored by thin layer chromatography (TLC) on 0.25 mm silica gel plates (GF-2.5). Melting points of all the compounds were detected by a MP50 Melting Point System. A Bruker AV-300

instrument was used to determine the $^{1}$H-NMR and $^{13}$C-NMR, deuterated solvents with tetramethysilane (TMS) as internal standard. ESI-MS and high-resolution mass spectra (HRMS) results of all the compounds were recorded on a Water Q-Tof micro mass spectrometer (all data were within 0.4 % of the theoretical values). The purity (≥95%) of the compounds was determined by the HPLC on an Agilent C18 column (4.6 mm × 150 mm, 3.5 μm) using a mixture of solvent containing methanol/water at a flow rate of 0.5 mL/min and the peaks were determined at 254 nm under UV.

## Chemistry

**Scheme 1. Synthetic Route of Compounds 12 a-i.**

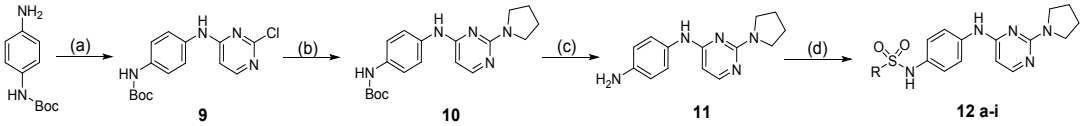


Reagents and conditions: (a) 2,4-dichloropyrimidine, *i*-PrOH, DIPEA, 80 °C, 10 h, 72%; (b) tetrahydropyrrole, 1,4-dioxane, DIPEA, 60 °C, 6 h, 93%; (c) $CF_3COOH$, DCM, rt, 70%; (d) different substituted sulfonyl chloride, toluene or DCM, TEA, rt, 65%.

**General procedures for the synthesis of 9-11**. 2,4-dichloropyrimidine (3g, 20 mmol) and tert-butyl (4-aminophenyl) carbamate were dissolved in the solution of *i*-PrOH (20 mL) and DIPEA (1mL) to react for 10 h at 80 °C. The reaction solvent was concentrated to 2 ml by rotary evaporator below 40 °C under reduced pressure before adding 50 mL water to make product precipitated. The product was filtered and washed with 50 mL water, then dried overnight in a vacuum desiccator, yielding **9** as a white solid. Then, **9** (1g, 3 mmol) was dissolved in the solution of 1,4-dioxane (15 mL) and DIPEA (0.5 mL) before tetrahydropyrrole (350 mg, 5 mmol) was added. The reaction was carried out at 60 °C for 6 h and then the solvent was removed by rotary evaporator below 60 °C under reduced pressure. The oily crude product was the dissolved in 1 mL DMF before adding 50 mL water to make product precipitated.

Crude product of **10** was filtered and washed with 50 mL water, then dried overnight in a vacuum desiccator. Finally, **10** (700 mg, 2 mmol) was dissolved in DCM (15 mL) and followed by adding trifluoroacetic acid (1 mL) to react for 4 h at room temperature. Then the solvent in the reaction mixture was removed by rotary evaporator below 40 °C under reduced pressure to obtain white solid as the final product **11** and dried overnight in a vacuum desiccator.

***tert*-butyl (4-((2-chloropyrimidin-4-yl)amino)phenyl) carbamate (9):** Yield: 72% as white solid. Mp 142-143 °C. $^1$H-NMR (300 MHz, DMSO, $\delta$) 9.58 (s, 1H), 7.88 (s, 1H), 7.41 (d, 2H, $J$ = 6.0Hz), 7.20 (d, 2H, $J$ = 8.36Hz), 6.10 (d, 1H, $J$ = 4.52 Hz), 1.62 (s, 9H). HRMS (ESI): found 321.7863 ($C_{15}H_{17}ClN_4O_2$, $[M+H]^+$, requires 321.7819).

***tert*-butyl (4-((2-(pyrrolidin-1-yl)pyrimidin-4-yl)amino)phenyl)carbamate (10):** Yield 93% as light yellow solid; Mp 162-163 °C; $^1$H-NMR (300 MHz, DMSO, $\delta$) 9.63 (s, 1H), 7.78 (d, 1H, $J$ = 4.52 Hz), 7.47 (d, 2H, $J$ = 4.36 Hz), 7.26 (d, 2H, $J$ = 6.06Hz), 5.93 (d, 1H, $J$ = 3.12 Hz), 3.18 (m, 4H), 2.01 (m, 4H), 1.42 (s, 9H). HRMS (ESI): found 356.4432 ($C_{19}H_{25}N_5O_2$, $[M+H]^+$, requires 356.4498).

***N*$^1$-(2-(pyrrolidin-1-yl)pyrimidin-4-yl)benzene-1,4-diamine (11):** Yield 70% as white solid; Mp 151-153 °C; $^1$H-NMR (300 MHz, DMSO, $\delta$) 7.83(d, 1H, $J$ = 3.64 Hz), 7.07 (d, 2H, $J$ = 8.42 Hz), 6.26 (d, 2H, $J$ = 7.22 Hz), 5.91 (d, 1H, $J$ = 3.2 Hz), 4.38 (s, 2H), 3.12 (m, 4H), 1.88 (m, 4H). HRMS (ESI): found 256.3282 ($C_{14}H_{17}N_5$, $[M+H]^+$, requires 256.3277).

**General procedures for preparation of 12 a-g. 11** (500 mg, 2 mmol) was dissolved in the solution of toluene (10 mL) and TEA (0.5 mL) before different benzensulfonyl chloride was added, respectively, including 4-(trifluoromethyl)-benzenesulfonyl chloride (488 mg, 2 mmol) to obtain **12a**, naphthalene-2-sulfonyl chloride (453 mg, 2 mmol) to obtain **12b**, 2,4,6-trimethylbenzenesulfonyl chloride (440 mg, 2 mmol) to obtain **12c**, 4-methoxybenzenesulfonyl chloride (412 mg, 2 mmol) to obtain **12d**, 4-(tert-butyl)benzenesulfonyl chloride (464 mg, 2 mmol) to obtain **12e**,

2,4-dimethoxybenzenesulfonyl chloride (472 mg, 2 mmol) to obtain **12f** and 2,5-dimethoxybenzenesulfonyl chloride (472 mg, 2 mmol) to obtain **12g**. The reaction was carried out at room temperature until the crude solid was precipitated. The final product was filtered and washed with 50 mL water, then dried overnight in a vacuum desiccator, yielding **12 a-g** (55%-88%).

***N*-(4-((2-(pyrrolidin-1-yl)pyrimidin-4-yl)amino)phenyl)-4-(trifluoromethyl) benzenesulfonamide (12a):** Yield 64% as light yellow solid; Mp 236-237 °C; $^1$H NMR (300 MHz, DMSO) $\delta$ 10.20 (s, 2H), 8.86 (s, 1H), 7.96 (d, $J$ = 8.6 Hz, 2H), 7.90 (d, $J$ = 8.7 Hz, 2H), 7.47 (d, $J$ = 8.7 Hz, 2H), 6.95 (d, $J$ = 8.7 Hz, 2H), 5.45 (s, 1H), 2.25 (s, 4H), 1.89 (s, 4H). HRMS (ESI): found 464.4856 ($C_{21}H_{20}F_3N_5O_2S$, $[M+H]^+$, requires 464.4852). HPLC (90:10 methanol:water with 1‰ TFA): $t_R$= 3.87 min, 97.85%.

***N*-(4-((2-(pyrrolidin-1-yl)pyrimidin-4-yl)amino)phenyl)naphthalene-2-sulfona mide (12b):** Yield 55% as yellow solid; Mp 252-254 °C; $^1$H NMR (300 MHz, DMSO) $\delta$ 10.07 (s, 1H), 8.87 (s, 1H), 8.36 (s, 1H), 8.10 (t, J = 8.0 Hz, 2H), 8.00 (d, $J$ = 7.6 Hz, 1H), 7.74 (m, 4H), 7.38 (m, 2H), 6.98 (d, $J$ = 8.7 Hz, 2H), 5.54 (s, 1H), 3.24 (m, 4H), 1.89 (s, 4H). HRMS (ESI): found 446.1578 ($C_{24}H_{23}N_5O_2S$ $[M+H]^+$, requires 446.1572). HPLC (90:10 methanol:water with 1‰ TFA): $t_R$= 4.21 min, 96.43%.

**2,4,6-trimethyl-*N*-(4-((2-(pyrrolidin-1-yl)pyrimidin-4-yl)amino)phenyl) benzenesulfonamide (12c):** Yield 55% as yellow solid; Mp 189-191 °C; $^1$H NMR (300 MHz, DMSO) $\delta$ 10.10 (s, 1H), 7.88 (d, $J$ = 3.52 Hz, 1H), 7.23 (s, 2H), 7.08 (d, $J$ = 3.0 Hz, 2H), 6.88 (d, $J$ = 5.84 Hz, 2H), 6.04 (d, $J$ = 4.32 Hz, 1H), 3.27 (m, 4H), 1.74 (m, 4H). HRMS (ESI): found 438.1898 ($C_{24}H_{27}N_5O_2S$ $[M+H]^+$, requires 438.1885). HPLC (90:10 methanol:water with 1‰ TFA): $t_R$= 3.64 min, 96.12%.

**4-methoxy-*N*-(4-((2-(pyrrolidin-1-yl)pyrimidin-4-yl)amino)phenyl) benzenesulfonamide (12d):** Yield 88% as light grey solid; Mp 213-215 °C; $^1$H NMR (300 MHz, DMSO) $\delta$ 9.80 (s, 1H), 8.89 (s, 1H), 8.08 (s, 1H), 7.63 (d, $J$ = 9.0 Hz, 2H), 7.40 (d, $J$ = 9.0 Hz, 2H), 7.03 (d, $J$ = 9.0 Hz, 2H), 6.93 (d, $J$ = 9.0 Hz, 2H), 5.57 (s, 1H), 3.78 (s, 3H), 1.89 (m, 4H). HRMS (ESI): found 426.1527 ($C_{21}H_{23}N_5O_3S$

[M+H]$^+$, requires 426.1522). HPLC (90:10 methanol:water with 1‰ TFA): $t_R$= 3.87 min, 97.85%.

**4-(*tert-butyl*)-*N*-(4-((2-(pyrrolidin-1-yl)pyrimidin-4-yl)amino)phenyl) benzenesulfonamide (12e):** Yield 62% as white solid; Mp 217-219 °C; $^1$H NMR (300 MHz, DMSO) $\delta$ 9.95 (s, 1H), 8.91 (s, 1H), 8.08 (s, 1H), 7.66 (d, $J$ = 8.4 Hz, 2H), 7.56 (d, $J$ = 8.4 Hz, 2H), 7.41 (d, $J$ = 8.8 Hz, 2H), 6.99 (d, $J$ = 8.7 Hz, 2H), 5.58 (s, 1H), 1.90 (s, 4H), 1.26 (s, 9H). HRMS (ESI): found 452.2049 ($C_{24}H_{29}N_5O_2S$ [M+H]$^+$, requires 452.2042). HPLC (90:10 methanol:water with 1‰ TFA): $t_R$= 4.13 min, 98.42%.

**2,4-dimethoxy-*N*-(4-((2-(pyrrolidin-1-yl)pyrimidin-4-yl)amino)phenyl) benzenesulfonamide (12f):** Yield 61% as white solid; Mp 225-226 °C; $^1$H NMR (300 MHz, DMSO) $\delta$ 9.53 (s, 1H), 8.84 (s, 1H), 8.07 (s, 1H), 7.59 (d, $J$ = 8.6 Hz, 1H), 7.35 (d, $J$ = 8.8 Hz, 2H), 6.95 (d, $J$ = 8.7 Hz, 2H), 6.64 (s, 1H), 6.54 (d, $J$ = 8.8 Hz, 1H), 5.55 (s, 1H), 3.90 (s, 3H), 3.79 (s, 3H), 1.90 (s, 4H). HRMS (ESI): found 456.1641 ($C_{22}H_{25}N_5O_4S$ [M+H]$^+$, requires 456.1627). HPLC (90:10 methanol:water with 1‰ TFA): $t_R$= 4.03 min, 97.66%.

**2,5-dimethoxy-*N*-(4-((2-(pyrrolidin-1-yl)pyrimidin-4-yl)amino)phenyl) benzenesulfonamide (12g):** Yield 58% as white solid; Mp 228-229 °C; $^1$H NMR (300 MHz, DMSO) $\delta$ 9.68 (s, 1H), 8.87 (s, 1H), 8.07 (s, 1H), 7.38 (d, $J$ = 8.3 Hz, 2H), 7.17 (s, 1H), 7.12 (s, 1H), 6.98 (d, $J$ = 8.2 Hz, 2H), 5.56 (s, 1H), 3.86 (s, 3H), 3.69 (s, 3H), 3.34 – 3.23 (m, 4H), 1.90 (s, 4H). HRMS (ESI): found 456.1630 ($C_{22}H_{25}N_5O_4S$ [M+H]$^+$, requires 456.1627). HPLC (90:10 methanol:water with 1‰ TFA): $t_R$= 4.09 min, 96.85%.

**Scheme 2. Synthetic Route of Compounds 15a-g.**

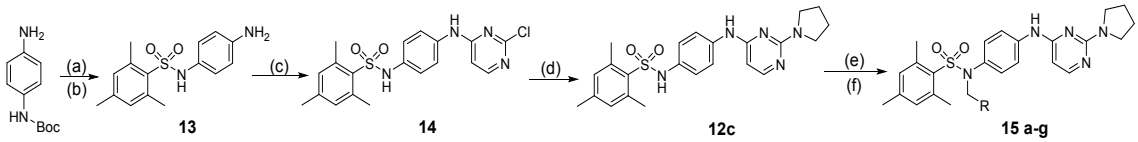

Reagents and conditions: (a) 2,4,6-trimethylbenzenesulfonyl chloride, toluene, TEA, rt, 86%; (b) $CF_3COOH$, DCM, rt, 70%; (c) 2,4-dichloropyrimidine, *i*-PrOH, DIPEA, 80 °C, 10 h, 72%; (d) tetrahydropyrrole, 1,4-dioxane, DIPEA, 60 °C, 6 h, 93%; (e) different substituted bromobenzene, DMF, $K_2CO_3$, rt, 73%; (f) $NaOH/H_2O$, rt, 89%.

**General procedures for the synthesis of 13,14 and 12c.** The tert-butyl (4-aminophenyl) carbamate (3g, 15 mmol) was directly dissolved in the solution of toluene (20 mL) and TEA (1 mL) before 2,4,6-trimethylbenzenesulfonyl chloride (2.2 g, 10 mmol) was added. Then the reaction was carried out at room temperature for 6 h until the light purple solid was precipitated. The crude product was filtered and directly dissolved in the solution of DCM (20 mL) and TFA (2 mL) for reacting at room temperature, 4 h. The mixture was concentrated and recrystallized with ethanol to afford the solid **13**. Subsequently, **13** (580 mg, 2mmol) was dissolved in the solution of *i*-PrOH (10 mL) and DIPEA (0.5 mL) before 2,4-dichloropyrimidine (300 mg, 2 mmol) was added. Then the mixture was stirred at 80 °C for 10 h. After cooling to the room temperature, the mixture was concentrated to 2 mL before 50 mL water was added. The precipitation was filtered and wash by 100 mL water to obtain **14**. Finally, **14** (1.2g, 3 mmol) was dissolved in the solution of 1,4-dioxane (15 mL) and DIPEA (0.5 mL) before tetrahydropyrrole (350 mg, 5 mmol) was added. The reaction was carried out at 60 °C for 6 h and then the solvent was removed by rotary evaporator below 60 °C under reduced pressure. The oiled crude product was the dissolved in 1 mL DMF before adding 50 mL water to make product precipitated. Crude product of **12c** was filtered and washed with 50 mL water, then dried overnight in a vacuum desiccator.

***N*-(4-aminophenyl)-2,4,6-trimethylbenzene-sulfonamide (13):** Yield 51% as white solid; Mp 163-164 °C; $^1$H NMR (300 MHz, DMSO) $\delta$ 10.30 (s, 1H), 7.33 (s, 2H), 6.98 (d, $J$ = 7.6 Hz, 2H), 6.44 (d, $J$ = 7.6 Hz, 2H), 4.46 (s, 2H), 2.71 (s, 6H), 2.09 (s, 3H). HRMS (ESI): found 291.3861 ($C_{15}H_{18}N_2O_2S$ $[M+H]^+$, requires 291.3860).

***N*-(4-((2-chloropyrimidin-4-yl)amino)phenyl)-2,4,6-trimethylbenzene-sulfona**

**mide (14):** Yield 72% as white solid; Mp 161-162 °C; $^1$H NMR (300 MHz, DMSO) $\delta$ 10.84 (s, 1H), 7.98 (d, $J$ = 8.5 Hz, 1H), 7.43 (s, 2H), 7.09 (d, $J$ = 6.0 Hz, 2H), 6.84 (d, $J$ = 3.0 Hz, 2H), 6.55 (d, $J$ = 7.6 Hz, 1H), 6.04 (s, 1H), 2.69 (s, 6H), 2.06 (s, 3H). HRMS (ESI): found 403.9016 ($C_{19}H_{19}ClN_4O_2S$ $[M+H]^+$, requires 403.9014).

**General procedures for 15a-g. 12c** (880 mg, 2 mmol) was dissolved in DMF (10 mL) with $K_2CO_3$ (560 mg, 2 mmol) added. Then, methyl 2-bromoacetate (765 mg, 3 mmol), was added dropwise under ice bath condition to room temperature. After the reaction, 100 mL water was added to obtain precipitation as crude product, filtered and washed by 100 mL water, yielding **15a**. **15b** was synthesized as previously reported. 2-bromoacetamide (414 mg, 3 mmol) was used to obtain **15c** and the procedure was similar as **15a**. 4-(bromomethyl)benzoic acid (645 mg, 3 mmol), 1-(bromomethyl)-4-isopropylbenzene (639 mg, 3 mmol), 1-(bromomethyl)-4-chlorobenzene (615 mg, 3 mmol) and 1-(bromomethyl)-4-methoxybenzene (603 mg, 3 mmol) were used to obtain **15d-g**, separately.

**methyl *N*-(mesitylsulfonyl)-*N*-(4-((2-(pyrrolidin-1-yl)pyrimidin-4-yl)amino) phenyl)glycinate (15a):** Yield 79% as white solid; Mp 235-236 °C; $^1$H NMR (300 MHz, DMSO-$d_6$) $\delta$ 9.40 (s, 1H), 7.87 (d, $J$ = 5.6 Hz, 1H), 7.62 (d, $J$ = 8.8 Hz, 2H), 7.10 (d, $J$ = 8.8 Hz, 2H), 6.94 (s, 2H), 6.02 (d, $J$ = 5.6 Hz, 1H), 4.00 (s, 2H), 3.68 (s, 3H), 2.38 (s, 5H), 2.23 (s, 3H), 1.91 (d, $J$ = 6.2 Hz, 4H). HRMS (ESI): found 510.2085 ($C_{26}H_{31}N_5O_4S$ $[M+H]^+$, requires 510.2097). HPLC (80:20 methanol:water with 1‰ TFA): $t_R$= 3.62 min, 96.32%.

***N*-(mesitylsulfonyl)-*N*-(4-((2-(pyrrolidin-1-yl)pyrimidin-4-yl)amino)phenyl) glycine (15b, DDO-5936):** the same as previously reported.

**2-((2,4,6-trimethyl-*N*-(4-((2-(pyrrolidin-1-yl)pyrimidin-4-yl)amino)phenyl) phenyl)sulfonamido)acetamide (15c):** Yield 73% as light yellow solid; Mp 235-236 °C; $^1$H NMR (300 MHz, DMSO-$d_6$) $\delta$ 8.94 (s, 1H), 8.15 (s, 1H), 7.38 (d, $J$ = 6.2 Hz, 2H), 7.17 (s, 1H), 7.01 (m, 6H), 5.53 (s, 1H), 4.14 (s, 2H), 3.23 (s, 4H), 2.14 (s, 6H), 2.03 (s, 3H), 1.81 (m, 4H). HRMS (ESI): found 495.2136 ($C_{25}H_{30}N_6O_3S$

[M+H]$^+$, requires 495.2138). HPLC (90:10 methanol:water with 1‰ TFA): $t_R$= 7.96 min, 96.37%.

**4-(((2,4,6-trimethyl-*N*-(4-((2-(pyrrolidin-1-yl)pyrimidin-4-yl)amino)phenyl) phenyl)sulfonamido)methyl)benzoic acid (15d):** Yield 43% as white solid; Mp 261-262 °C; $^1$H NMR (300 MHz, $CDCl_3$) δ 10.31 (s, 1H), 8.10 (s, 1H), 7.54 (s, 1H), 7.27 (m, 2H), 7.07 (d, *J* = 9.0 Hz, 1H), 6.95 (d, *J* = 9.0 Hz, 2H), 6.90 (m, 4H), 5.57 (d, *J* = 6.2 Hz, 1H), 4.80 (s, 3H), 2.51 (s, 6H), 2.29 (s, 3H), 1.98 (m, 4H). HRMS (ESI): found 572.2258 ($C_{31}H_{33}N_5O_4S$ [M+H]$^+$, requires 572.2253). HPLC (90:10 methanol:water with 1‰ TFA): $t_R$= 5.24 min, 98.24%.

***N*-(4-isopropylbenzyl)-2,4,6-trimethyl-*N*-(4-((2-(pyrrolidin-1-yl)pyrimidin-4-yl )amino)phenyl)benzenesulfonamide (15e):** Yield 53% as white solid; Mp 250-251 °C; $^1$H NMR (300 MHz, $CDCl_3$) δ 8.21 (s, 1H), 7.27 (s, 1H), 7.12 (d, *J* = 3.0 Hz, 1H), 7.09 (m, 4H), 7.00 (m, 3H), 6.95 (d, *J* = 9.0 Hz, 2H), 5.6 (s, 1H), 4.78 (s, 2H), 3.39 (s, 4H), 2.86 (m, 1H), 2.82 (s, 6H), 2.51 (s, 3H), 2.01 (m, 4H), 1.27 (s, 6H). HRMS (ESI): found 570.2027 ($C_{33}H_{39}N_5O_2S$ [M+H]$^+$, requires 570.2011). HPLC (90:10 methanol:water with 1‰ TFA): $t_R$= 5.69 min, 98.61%.

***N*-(4-chlorobenzyl)-2,4,6-trimethyl-*N*-(4-((2-(pyrrolidin-1-yl)pyrimidin-4-yl)a mino)phenyl)benzenesulfonamide (15f):** Yield 67% as white solid; Mp 259-260 °C; $^1$H NMR (300 MHz, $CDCl_3$) *δ* 8.21 (s, 1H), 7.22 (m, 5H), 7.17 (m, 2H), 7.14 (m, 4H), 6.93 (m, 4H), 5.57 (s, 1H), 4.78 (s, 1H), 4.45 (s, 2H), 3.48 (s, 1H), 2.48 (s, 6H), 2.28 (s, 3H), 2.01 (m, 4H). HRMS (ESI): found 562.1938 ($C_{30}H_{32}ClN_5O_2S$ [M+H]$^+$, requires 562.1965). HPLC (90:10 methanol:water with 1‰ TFA): $t_R$= 5.67 min, 95.97%.

***N*-(4-methoxybenzyl)-2,4,6-trimethyl-*N*-(4-((2-(pyrrolidin-1-yl)pyrimidin-4-yl) amino)phenyl)benzenesulfonamide (15g):** Yield 63% as white solid; Mp 248-249 °C; $^1$H NMR (300 MHz, $CDCl_3$) δ 8.12 (s, 1H), 7.02 (m, 4H), 6.88 (m, 5H), 6.67 (d, *J* = 9.0 Hz, 2H), 5.50 (s, 1H), 4.66 (s, 2H), 3.66 (s, 3H), 3.39 (s, 3H), 2.41 (s, 6H), 2.19 (s, 3H), 2.08 (s, 1H), 1.90 (m, 4H). HRMS (ESI): found 558.2451 ($C_{30}H_{32}ClN_5O_2S$ [M+H]$^+$, requires 558.2461). HPLC (90:10 methanol:water with 1‰

TFA): $t_R$= 5.84 min, 97.62%.

**Scheme 3. Synthetic Route of Compounds 17a-i and 18a-i.**

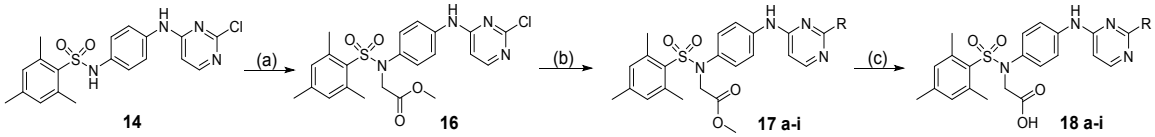


Reagents and conditions: (a) methyl bromoacetate, DMF, $K_2CO_3$, rt, 73%; (b) different amine, 1,4-dioxane, DIPEA, 60 °C, 6 h; (c) methanol, NaOH/$H_2O$, rt.

**Preparation of methyl *N*-(4-((2-chloropyrimidin-4-yl)amino) phenyl)-*N*-(mesitylsulfonyl) glycinate (16): 14** (800 mg, 2 mmol) was dissolved in DMF (10 mL) with $K_2CO_3$ (560 mg, 2 mmol) added. Then, methyl 2-bromoacetate (765 mg, 5 mmol) was added dropwise under ice bath condition to room temperature. After the reaction, 100 mL water was added to obtain precipitation as crude product, filtered and washed by 100 mL water to afford **16**: Yield 69% as light grey solid; Mp 211-212 °C; $^1$H NMR (300 MHz, DMSO-$d_6$) $\delta$ 7.89 (d, $J$ = 5.6 Hz, 1H), 7.26 (s, 2H), 7.13 (d, $J$ = 8.6 Hz, 2H), 6.64 (d, $J$ = 9.0 Hz, 2H), 6.32 (d, $J$ = 7.2 Hz, 1H), 4.82 (s, 1H), 3.51 (s, 3H), 2.63 (s, 6H), 2.10 (s, 3H). HRMS (ESI): found 475.9632 ([M+H]$^+$, requires 475.9630).

**General procedure for 18a-i.** Intermediate **16** (950 mg, 2 mmol) was dissolved in the mixture of 1,4-dioxane of DIPEA. Then, different amines (3 mmol) were added and stirred at 80 °C for 8 h under a nitrogen atmosphere. After confirming the results of the reactions by TLC, the final mixtures were concentrated and subsequently purified by normal phase column chromatography (DCM: methanol 10:1) to separately afford **17a-i**. Next, **17a-i** were directly dissolved in solution containing 10 M NaOH/$H_2O$ and stirred at room temperature. After the reaction, pH was adjusted to 7, resulting crude product precipitated. Then the mixture was filtered and washed with water for 5 times to afford **18a-i**.

***N*-(mesitylsulfonyl)-*N*-(4-((2-(methylamino)pyrimidin-4-yl)amino)phenyl)glycine (18a):** Yield 57% as yellow solid; Mp 204-205 °C; $^1$H NMR (300 MHz, DMSO-$d_6$) $\delta$10.02 (s, 1H), 7.87 (d, $J$ = 6.11 Hz, 1H), 7.69 (d, $J$ = 8.39 Hz, 2H), 7.44 (s, 1H), 7.17 (d, $J$ = 8.39 Hz, 2H), 7.01 (s, 2H), 6.14 (d, $J$ = 6.15 Hz, 1H), 4.46 (s, 2H), 2.83 (d, $J$ = 4.59 Hz, 3H), 2.53 (s, 6H), 2.26 (s, 3H). HRMS (ESI): found 456.1709 ($C_{22}H_{25}N_5O_4S$ $[M+H]^+$, requires 456.5330). HPLC (80:20 methanol:water with 1‰ TFA): $t_R$= 7.41 min, 95.89%.

***N*-(4-((2-(ethylamino)pyrimidin-4-yl)amino)phenyl)-*N*-(mesitylsulfonyl)glycine (18b):** Yield 37% as gray solid; Mp 207-208 °C; $^1$H NMR (300 MHz, DMSO-$d_6$) $\delta$9.23 (s, 1H), 7.84 (d, $J$ = 5.58 Hz, 1H), 7.61 (d, $J$ = 8.45 Hz, 2H), 7.12 (d, $J$ = 8.73 Hz, 2H), 6.97 (s, 2H), 5.97 (d, $J$ = 5.64 Hz, 1H), 4.04 (s, 2H), 2.41 (s,6H), 2.26 (s, 3H), 1.28 (m, 2H), 1.12 (t, 3H). HRMS (ESI): found 470.1864 ($C_{23}H_{27}N_5O_4S$ $[M+H]^+$, requires 470.5624). HPLC (80:20 methanol:water with 1‰ TFA): $t_R$= 8.50 min, 96.79%.

***N*-(4-((2-(cyclopropylamino)pyrimidin-4-yl)amino)phenyl)-*N*-(mesitylsulfonyl)glycine (18c):** Yield 29% as light gray solid; Mp 214-215 °C; $^1$H NMR (300 MHz, DMSO-$d_6$) δ7.75 (d, J = 6.17 Hz, 1H), 7.27 (s, 4H), 7.02 (s, 2H), 5.48 (d, J = 5.98 Hz, 1H), 4.47 (d, J = 3.46 Hz, 4H), 2.36 (s,6H), 2.25 (s, 3H), 0.61 (m, 2H), 0.43 (m, 2H). HPLC (80:20 methanol:water with 1‰ TFA): $t_R$= 9.29 min, 95.17%. HRMS (ESI): found 482.5787 ($C_{24}H_{27}N_5O_4S$ $[M+H]^+$, requires 482.5702).

***N*-(mesitylsulfonyl)-*N*-(4-((2-(pentan-3-ylamino)pyrimidin-4-yl)amino)phenyl)glycine (18d):** Yield 64% as white solid; Mp 217-218 °C; $^1$H NMR (300 MHz, DMSO-$d_6$) δ9.37 (s, 1H), 7.88 (d, $J$ = 5.69Hz, 1H), 7.63 (d, $J$ = 8.73Hz, 2H), 7.10 (d, $J$ = 8.69Hz, 2H), 6.97 (s, 2H), 5.99 (d, $J$ = 5.85Hz, 1H), 4.41 (s, 2H), 3.44 (t, 6H), 2.33 (s, 6H), 2.23 (s, 3H), 1.90 (t, 4H). HRMS (ESI): found 512.6232 ($C_{26}H_{33}N_5O_4S$ $[M+H]^+$, requires 512.6297). HPLC (80:20 methanol:water with 1‰ TFA): $t_R$= 11.37 min, 97.83%.

***N*-(4-((2-(diethylamino)pyrimidin-4-yl)amino)phenyl)-*N*-(mesitylsulfonyl)glycine (18e):** Yield 59% as white solid; Mp 211-212 °C; $^1$H NMR (300 MHz,

DMSO-$d_6$) $\delta$ 9.22 (s, 1H), 7.89 (d, $J$ = 5.49 Hz, 1H), 7.56 (d, $J$ = 9.00 Hz, 2H), 7.06 (d, $J$ = 8.89 Hz, 2H), 6.96 (s, 2H), 5.94 (d, $J$ = 5.54 Hz, 1H), 4.39 (s, 2H), 3.51 (m, 4H), 2.32 (s, 6H), 2.22 (s, 3H), 1.08 (t, 6H). HRMS (ESI): found 498.2177 ($C_{25}H_{31}N_5O_4S$ $[M+H]^+$, requires 498.6129). HPLC (80:20 methanol:water with 1‰ TFA): $t_R$= 5.32 min, 96.10%.

***N*-(mesitylsulfonyl)-*N*-(4-((2-(piperidin-1-yl)pyrimidin-4-yl)amino)phenyl)glycine (18f):** Yield 74% as white solid; Mp 219-220 °C; $^1$H NMR (300 MHz, DMSO-$d_6$) $\delta$ 12.73 (s, 1H), 7.84 (d, $J$ = 5.70 Hz, 1H), 7.31 (s, 4H), 7.06 (s, 2H), 5.48 (d, $J$ = 5.88 Hz, 1H), 4.52 (s, 2H), 3.68 (t, 4H), 2.40 (s, 6H), 2.29 (s, 3H), 1.63 (s, 2H), 1.49 (s, 4H). HRMS (ESI): found 510.2934 ($C_{26}H_{31}N_5O_4S$ $[M+H]^+$, requires 510.6217). HPLC (80:20 methanol:water with 1‰ TFA): $t_R$= 8.49 min, 98.42%.

***N*-(4-((2-(azepan-1-yl)pyrimidin-4-yl)amino)phenyl)-*N*-(mesitylsulfonyl)glycine (18g):** Yield 61% as white solid; Mp 224-225 °C; $^1$H NMR (300 MHz, DMSO-$d_6$) $\delta$ 9.26 (s, 1H), 7.89 (d, $J$ = 5.60 Hz, 1H), 7.56 (d, $J$ = 8.75Hz, 2H), 7.06 (d, $J$ = 8.90 Hz, 2H), 6.97 (s, 2H), 6.72(s, 1H), 5.95 (d, $J$ = 5.43 Hz, 1H), 4.42 (s, 2H), 3.62 (s, 4H), 2.33 (s, 6H), 2.23 (s, 3H), 1.67 (s,4H), 1.47(s, 4H). HRMS (ESI): found 524.2331 ($C_{27}H_{33}N_5O_4S$ $[M+H]^+$, requires 524.6570). HPLC (80:20 methanol:water with 1‰ TFA): $t_R$= 9.64 min, 96.06%.

***N*-(mesitylsulfonyl)-*N*-(4-((2-(piperazin-1-yl)pyrimidin-4-yl)amino)phenyl)glycine (18h):** Yield 35% as light yellow solid; Mp 242-243 °C;$^1$H NMR (300 MHz, DMSO-$d_6$) $\delta$ 9.65 (s, 1H), 7.97 (d, $J$ = 6.32, 1H), 7.65 (d, $J$ = 8.06, 2H), 7.28 (d, $J$ = 8.69, 2H), 7.04 (s, 2H), 5.98 (d, $J$ = 5.70, 1H), 4.61 (s, 2H), 4.04 (s, 4H), 3.27 (s, 4H), 2.38 (s, 6H), 2.28 (s, 3H). $^{13}$C NMR (75 MHz, DMSO-$d_6$) $\delta$ 171.45, 160.94, 160.37, 156.15, 142.33, 140.06, 139.78, 133.34, 133.14, 131.94, 129.93, 119.11, 98.17, 43.26, 41.64, 22.95, 20.88. HRMS (ESI): found 511.2123 ($C_{25}H_{30}N_6O_4S$ $[M+H]^+$, requires 511.6110). HPLC (80:20 methanol:water with 1‰ TFA): $t_R$= 4.89 min, 98.45%.

***N*-(mesitylsulfonyl)-*N*-(4-((2-(4-methylpiperazin-1-yl)pyrimidin-4-yl)amino)phenyl)glycine (18i):** Yield 61% as light yellow solid; Mp 239-240 °C; $^1$H NMR (300 MHz, DMSO-$d_6$) $\delta$ 9.23 (s, 1H), 7.88 – 7.66 (m, 1H), 7.40 (d, $J$ = 8.1 Hz, 2H),

7.14 – 6.89 (m, 2H), 6.86 (s, 2H), 6.00 – 5.83 (m, 1H), 4.19 (s, 2H), 3.53 (s, 4H), 2.33 (s, 3H), 2.25 (s, 6H), 2.14 (d, *J* = 7.4 Hz, 4H). HRMS (ESI): found 525.2214 ($C_{26}H_{32}N_6O_4S$ $[M+H]^+$, requires 525.2217). HPLC (80:20 methanol:water with 1‰ TFA): $t_R$= 7.18 min, 96.37%.

**Scheme 4. Synthetic Route of Compounds 19-21.**

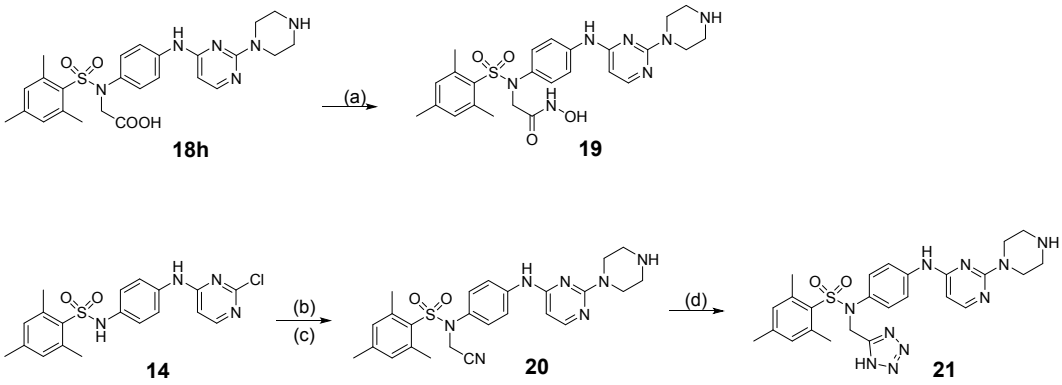


Reagents and conditions: (a) Hydroxylamine, DIC, isopropanol, 45~55℃; (b) bromoacetonitrile, DMF, $K_2CO_3$, rt; (c) piperazine, DIPEA, *i*-PrOH, reflux; (d) $NaN_3$, $NH_4Cl$, reflux, 5h.

***N*-hydroxy-2-((2,4,6-trimethyl-*N*-(4-((2-(piperazin-1-yl)pyrimidin-4-yl)amino) phenyl)phenyl)sulfonamido)acetamide (19). 18h** (1g, 2 mmol) was dissolved in the mixture of isopropanol and dehydrant DIC (6 mmol). 10-folds of excessive amount of hydroxylamine was then added. The reaction was stirred at 60 $^{O}$C for about 24h to afford compound **19**. The crude product was concentrated and recrystallized using ethanol. Yielding 42% as white solid; Mp 253-254 °C; $^1$H NMR (300 MHz, DMSO-d6) *δ*9.61 (s, 1H), 7.98 (d, *J* = 6.63, 1H), 7.64 (d, *J* = 6.63, 2H), 7.27 (d, *J* = 8.65, 2H), 7.04 (s, 2H), 4.55 (s, 2H), 4.02 (s, 4H), 3.23 (S, 4H), 2.38 (s, 6H), 2.28 (s, 3H). HRMS (ESI): found 526.2283 ($C_{25}H_{31}N_7O_4S$ $[M+H]^+$, requires 526.2202). HPLC (80:20 methanol:water with 1‰ TFA): $t_R$= 7.64 min, 96.17%.

***N*-(cyanomethyl)-2,4,6-trimethyl-*N*-(4-((2-(piperazin-1-yl)pyrimidin-4-yl)amin o)phenyl)benzenesulfonamide (20). 14** (800mg, 2 mmol) was dissolved in DMF with (830 mg, 6 mmol) $K_2CO_3$. Then, bromoacetonitrile (0.2 ml, 3mmol) was added

dropwise at room temperature. After being detected by ITC, triple amount of water was added to obtain precipitation as crude product, which was then filtered and washed by 100 mL water. The intermediate was directly dissolved in the mixture of 1,4-dioxane with DIPEA in it and stirred with piperazine (4 mmol) at 80 $^{O}$C for 8h to afford crude product of **20**. The crude product was concentrated and purified by column chromatography (DCM: $CH_3OH$ = 100: 1) to obtain purified compound **20**. Yielding 77% as light brown solid; Mp 247-248 °C; $^1$H NMR (300 MHz, DMSO-$d_6$) $\delta$9.35 (s, 1H), 8.02 (d, $J$ = 6.52, 1H), 7.71 (d, $J$ = 8.31, 2H), 7.28 (d, $J$ = 8.79, 2H), 7.10 (s, 2H), 6.48 (d, $J$ = 6.39, 1H), 4.91 (s, 2H), 3.00 (s, 4H), 3.28 (s, 4H), 2.41 (s, 6H), 2.31 (s, 3H). HRMS (ESI): found 492.6129 ($C_{25}H_{29}N_7O_2S$ $[M+H]^+$, requires 492.6042). HPLC (80:20 methanol:water with 1‰ TFA): $t_R$= 3.87 min, 97.26%.

***N*-((1H-tetrazol-5-yl)methyl)-2,4,6-trimethyl-*N*-(4-((2-(piperazin-1-yl)pyrimidin-4-yl)amino)phenyl)benzenesulfonamide (21). 20** (980 mg, 2 mmol) was dissolved in DMF. Triple amount of $NaN_3$ (390 mg, 6 mmol) was added for a plurality of times, after which 4 folds amount of $NH_4Cl$ was subsequently added all at once. After adding 50 mL water to the mixture, **21** was afforded by filtering and washing. Yielding 25% as gray solid; Mp 234-235 °C; $^1$H NMR (300 MHz, DMSO-$d_6$) $\delta$9.52 (s, 1H), 8.13 (s, 1H), 8.01 (d, $J$ = 5.60, 1H), 7.63 (d, $J$ = 8.80, 2H), 7.16 (d, $J$ = 8.84, 2H), 7.07 (s, 2H), 6.11 (d, $J$ = 5.75, 1H), 4.89 (s, 2H), 3.72 (m, 4H), 3.47 (s, 4H), 2.39 (s, 6H), 2.29 (s, 3H). HRMS (ESI): found 535.6419 ($C_{25}H_{30}N_{10}O_2S$ $[M+H]^+$, requires 535.6427). HPLC (80:20 methanol: water with 1‰ TFA): $t_R$= 8.96 min, 95.10%.

**Molecular Docking and Molecular Dynamic (MD) Simulation.** The crystal structure of Hsp90-Cdc37 (PDB ID: 1US7) was downloaded from the Protein Data Bank (PDB). All the compounds and protein structures were imported to Discovery Studio (DS) 3.0 and the conformations were generated with the protocol “Prepare Protein” and “Prepare Ligands” respectively. Molecular Docking was performed using CDOCKER tool and the protein residues around the identified critical residues for Hsp90-Cdc37 PPI (including Glu47 and Gln133) were defined as the binding sites. Docking process was conducted with the default parameters without other

mentioned. The MD simulation analysis and MD trajectories were conducted as similar procedure as previous reported[32].

**Cloning, expression, and purification of recombinant Hsp90 and Cdc37.** The plasmid DNA of Hsp90 (the full-length and N-terminal residues including residues 9 to 236), Cdc37 and their site-directed mutants with R46A, E47A, Y61A, and Q133A in Hsp90 were cloned to carrier Pet28a. It was then transfected into an *Escherichia Coli* BL21 strain, which was incubated at 37°C in lysogeny broth medium with ampicillin (100 ug/ml) in it. When the optical density (OD) values reached 0.6~0.8, isopropyl β-D-1-thiogalactopyranoside (1 mM) was used to induce the expression of protein, which lasted for 20 hours. After centrifugation at 5000 rpm for 15 minutes, the cells were collected and stored at -80 °C. The purification of protein included the following steps: first, the colibacillus were suspended in lysis buffer (20 mM Tris-HCl, pH = 7.4, 200 mM NaCl and 1 mM dithiothreitol), which was then lysed by sonication, and centrifuged at 12,000 rpm for 30 min at 4 °C. The supernatant was collected and filtered with 0.45 μm syringe and then purified with a nickel column. Subsequently, the eluted proteins after the gel filtration on HiLoad 60 Superdex 200 columns (GE Healthcare) were analyzed by SDS-polyacrylamide gel electrophoresis (PAGE). All proteins were stored in phosphate-buffered saline (PBS) buffer at -80 °C.

**HTRF assay.** The standard method (www.cisbio.com) was followed here in HTRF assays. 4 μL of His-Hsp90 and 4 μL of GST-Cdc37 were premixed in PBS buffer with 200 mM KF (pH = 7.4), leading to a final concentration of 80 nM. Then 4 μL of diluted compounds solution was added and incubated for 1 hour at 37°C. 4 μL of anti-GST Cryptate (61GSTKLA, Cisbio) and 4 μL of anti-6HisXL665 (61HISXLA, Cisbio) were subsequently added, making a final volume of 20 μL. After another 30 minutes incubation at room temperature, the results were measured by a Molecular Devices instrument (SpectraMax Paradigm; excitation, 320 nm; emission, 665 nm and 620 nm). The final HTRF ratio was calculated as: ratio = (Signal 665 nm/Signal 620 nm) × 10,000.

**NMR assay.** Ligand-observed T1ρ and STD NMR experiments were used to

testify the interactions between the inhibitors and the proteins. All NMR spectra were obtained at 25 °C on a Bruker Avance III 600 MHz (proton frequency) spectrometer equipped with a cryogenically cooled probe (Bruker BioSpin, Germany). For ligand-observed T1ρ experiments, 200 μM compound along with 0, 1, 5 and 20 μM of Hsp90 was prepared as samples. While for the STD NMR experiments, 100 μM compound and 5 μM Hsp90 were prepared as samples. Compounds and proteins needed in the NMR assays were all dissolved in phosphate buffer (20 mM sodium phosphate, 150 mM NaCl, 5% DMSO, pH = 7.4).

**Biolayer interferometry assay.** Biolayer interferometry assays on Octet RED96 (ForteBio) were used to determine the dose-dependent binding affinities of the inhibitors for wild-type or mutant Hsp90. Proteins used in this assay were all biotinylated by EZ-Link NHS-Biotin (20217, Thermo Fisher Scientific). Super Streptavidin (SSA) biosensor tips (ForteBio Inc., Menlo Park, CA) that were prewetted with kinetic buffer (PBS, 0.05%; bovine serum albumin, 0.01% Tween 20) for 10 minutes were used in this assay to immobilize the Hsp90 (100 μg/mL). A new set of biosensors incubated in buffer without proteins was used as background controls. All the assays were conducted in 96-well black plates with the volume of 200 μL each well at 28°C. All the data were analyzed on Octet data analysis software. A double reference subtraction protocol was used to analyze the signals, which would reduce the influence of background and nonspecific signals. A 1:1 binding model was used in this assay and the equilibrium dissociation constant ($K_D$) values were calculated from the ratio of $K_{off}$ to $K_{on}$ ($K_D = K_{off}/K_{on}$).

**ITC assay.** ITC (MicroCal iTC200) was used to determine the binding affinities between Hsp90 and the synthesized compounds. Proteins with the concentration of 50 μM were prepared in the assay buffer (20 mM tris-HCl, 150 mM NaCl, pH = 7.4) and subsequently injected to in titration cells, and compounds with the concentration of 300 μM in the same assay buffer were in syringes. The whole injection procedure was set with intervals of 180 seconds and a stirring speed of 1000 rpm, involving 19 injections in total. In order to prevent interference and ensure the accuracy, the first

titration of the ligand solution was 0.5 μL. Origin software was finally used to analyze the data obtained to determine the binding parameters, including the enthalpy value (ΔH), entropy value (ΔS), and the association constant ($K_a = 1 / K_d$).

**Hsp90 ATPase assay.** A Discover RX ADP Hunter Plus Assay Kit (Discovery, Fremont, CA) was used here to conduct the Hsp90 ATPase assay. Tests were all carried out in 384-well black plates at 37°C, with each well containing 20 μL of indicated concentration of compound, 20 μL of Hsp90 protein (5 μM) and 20 μL of ATP (100 μM) and incubating for 1 hour. After that, 10 μL of detection reagent A and 20 μL of detection of reagent B were added and mixed homogeneously for a 30 mins incubation at room temperature. Subsequently, a Varioskan multimode microplate spectrophotometer (Thermo Scientific Varioskan) was used to detect the amount of ADP generated. Meanwhile, the background values were tested without proteins or compounds, and the negative control values were tested without compounds only, regarded as 100% protein activity.

**Thermal shift assay.** N-terminal of Hsp90 (10 μM) and the indicated concentrations of the inhibitors (200, 100, 50 and 10 μM) were mixed together in the assay buffer (1× PBS, pH = 8.0) respectively. Then, 6× SYPRO Orange dye (Thermo Fisher Scientific, UK) was added to make a final volume of 20 μL. 96-well polymerase chain reaction (PCR) plates were used in this assay, and a PCR system (StepOnePlus, Applied Biosystems) were used subsequently to heat the samples from room temperature to 99 °C with a rate of 1 °C/min. Fluorescence intensities were monitored at the condition of 492 nm excitation and 610 nm emission. Melting temperature ($T_m$) without the inhibitors (replaced by the same amount of DMSO) was used as control. $T_m$ values were obtained from the maximum value of first derivative ($dF/dT$) plots of the protein melting curves and were analyzed on Protein Thermal Shift software v1.3 (Thermo Fisher Scientific).

**In vitro antiproliferative assay.** Antiproliferative activities of all the compounds against different cell lines were determined using CCK8 assay kit. Firstly, cells were seeded into 96-well plates at 3000-5000 cells per well and incubated for 24 h.

Subsequently, serial dilutions of the compounds (the same amount of DMSO was used as control) were added in the plates for 72 h. Then, the cell proliferation was determined by CCK8 kit according to the standard protocol (Beyotime, Jiangsu, China).

**Plasma stability and microsomal stability.** Plasma stability was determined as following steps: (1) Prepare a 10mM DMSO stock of the testing compound. (2) Dilute the 10 mM stock to 1 μM by mouse or human plasma. (3) Transfer 50 μL plasma into a new tube and stop reaction by 250uL Acetonitrile. (4) Incubate the plasma sample in water bath at 37 $^{o}$C. (5) Stop reaction at 10 min, 30 min, 60 min and 90 min, respectively. (6) Measure the compound concentration by LC-MS/MS; Microsomal stability was determined using10 μM of **DDO-5936** and **18h** to incubate with human and mouse microsomes (0.5 mg/mL) for 5 min at 37 $^{o}$C in phosphate buffer (100 mM, pH = 7.4) before 1 mM NADPH was added to start the reaction. Then, the cold acetonitrile was utilized to precipitate the protein. Last, the samples were centrifuged for further analysis by LC-MS/MS.

**Pharmacokinetic Experiments.** The pharmacokinetics studies of the **DDO-5936** and **18h** were conducted in tumor xenograft model mice. The compounds (**DDO-5936** and **18h**) were orally administered (80mg/kg) to the mice, respectively. Blood samples and the tumor samples were collected into heparinized Eppendorf tubes at indicated time points (including 0, 0.25, 0.5, 1, 2, 4, 8, 12 and 24h). Finally, the plasma and the tumor samples were stored at -80 $^{o}$C for the analysis by LC-MS/MS.

**Cellular thermal shift assay (CETSA).** CETSAs were performed according to previously published standard protocols. HCT116 cells were seeded in 10 cm cell culture dishes to reach ~90% confluence. HCT116 cells were treated with 20 μM **18h** or the same amount of DMSO before they were collected and washed by PBS buffer for 3 times. The collected cells were isolated and resuspended in PBS buffer, which were equally distributed into 200 μL PCR tubes. The tubes were heated at the indicated temperature (37$^{o}$C to 75°C) to denature the samples for 3 minutes. Subsequently, the denatured cells were freeze-thawed three times in liquid nitrogen

before being centrifuged and analyzed by Western blot.

**Co-IP assay.** HCT116 cells were seeded in 10 cm cell culture dishes to reach ~90% confluence. Then, the cells and the indicated concentrations of compounds or the same volume of DMSO as controls were incubated together for 12 hours. After being washed twice by ice cold PBS, the cells were lysed by radio-immunoprecipitation assay (RIPA) buffer (50 mM tris, 150 mM NaCl, 1% NP-40 and protease inhibitor cocktail, Roche, pH =7.4) for 1 hour on ice, whose lysates were centrifuged at 12,000 rpm at 4°C for 15 minutes. Afterwards, 1 mg of cell lysates was incubated with 5 μg of anti-Hsp90 (sc-13119, Santa Cruz Biotechnology), anti-Cdc37 (4793S, Cell Signaling Technology), anti-CDK4 (ab199728, Abcam) or normal rabbit immunoglobulin G (IgG) (sc-2027, Santa Cruz Biotechnology) separately overnight at 4°C on a vertical roller. Another 3-hour incubation was continued after adding protein A/G Magnetic Agarose Beads (78609, Thermo Fisher Scientific) to lysates. Last, the beads were washed by RIPA buffer for 5 times and then subjected to SDS-PAGE, followed by western blot analysis.

**Immunoblotting and antibodies.** For Western blots, the proteins were prepared in 1× SDS loading buffer, and applied to SDS-PAGE and transferred to Immobilon-P$^{SQ}$ Transfer Membranes (Merck Millipore) which were afterwards blocked by 5% nonfat milk for 1 hour at room temperature. Then, specific primary antibodies were added and incubated overnight at 4°C. Horseradish peroxidase (HRP)–linked anti-rabbit IgG (catalog no. 7074P2, lot no. 26, Cell Signaling Technology) or HRP-linked anti-mouse IgG (catalog no. 7076P2, lot no. 32, Cell Signaling Technology) functioned as a secondary antibody. Subsequently, an Immobilon Western Chemiluminescent HRP Substrate Kit (Merck Millipore) were used to detect the protein bands.

**Cell cycle analysis.** Cells treated with the indicated concentrations of compounds were incubated at 37°C for 24 hours before being harvested and fixed with 75% ethanol overnight at 4°C. Cells were incubated with Ribonuclease I (50 μg/mL) in PBS at 37°C for 30 minutes, and stained by PI (50 μg/mL) for 15 minutes. Cell cycle

assays were performed on Flow cytometry and FACSDiva software, v 6.2 (BD Biosciences). FlowJo software was used to analyze the cell cycle phases.

**Cell culture.** HCT116, A549 and L02 cell lines were obtained from the Cell Resource Center of Shanghai Institute for Biological Sciences, Chinese Academy of Sciences. The cell lines used in this study were maintained in RPMI 1640 medium supplemented with 10% fetal bovine serum (FBS). All cells were authenticated by short tandem repeat profiling, examined for mycoplasma contamination, and cultured at 37°C in a humidified, 5% $CO_2$ containing atmosphere incubator (Thermo Fisher Scientific).

**Tumor xenograft experiments.** HCT116 cells ($1 \times 10^7$) and Matrigel (BD Biosciences) were mixed together in a 3:1 volume on ice and injected into the flanks of 6-week-old BALB/c nude mice which were randomly divided into three groups to generate xenografts. The treatment began when the mean tumor volumes reached 125 $mm^3$, and continued for 21 days, giving an oral administration of 0.9% saline solution containing 5% DMSO (vehicle) and compounds (**DDO-5936** and **18h**, 40 or 80 mg/kg) daily. By measuring the two perpendicular diameters of the tumors, the tumor volume was determined everyday (V = length (mm) × width $(mm)^2/2$), and the body weights were recorded every 3 days. After 21 days, the mice were sacrificed and dissected, whose tumor tissues and experimental organs were weighed and collected for further study. All animals used in this study were handled according to federal and institutional guidelines under a protocol approved by the Institutional Animal Care and Use Committee at China Pharmaceutical University.

**H&E staining and immunohistochemistry.** Tumor tissues and normal organs were immobilized in 4% formaldehyde solution and paraffin-embedded, which were then cut to make the thickness 4 μm and fixed on a glass slide to detect the morphology after being stained with H&E for imaging. For immunohistochemical staining, the tumor tissues were fixed by formalin and embedded by paraffin, sectioning into 4 μm slices. Then, the tissue sections were deparaffinized, rehydrated and 3% $H_2O_2$ was added to quench the endogenous peroxidase activity. Antigen

retrieval was carried out by boiling slides in sodium citrate buffer (10 mM, pH = 6.0). The immunohistochemistry reaction was determined by a DAB substrate kit. Briefly, the paraffin sections of different groups were deparaffinized, rehydrated and incubated in 3% hydrogen peroxide ($H_2O_2$). All the samples were incubated with the primary antibody (CDK4) at 4 °C overnight following a block process with 3% BSA. Then, secondary antibody was incubated for 20 min at 37 °C, respectively. Samples were stained with DAB and retained with hematoxylin. After dehydrated and dried, the sections were observed under a light microscopy (200 ×) (Nikon, Tokyo, Japan).

**Pharmacokinetics.** The xenograft model mice (n = 6 per group) were orally administered **DDO-5936** and **18h** at 80 mg/kg. 150 μL of blood samples at indicated time points (0, 0.25, 0.5 1, 2, 8, 12 and 24 hours) were collected in heparinized Eppendorf tubes to get plasma samples after being centrifuged at 3000 rpm for 10 minutes, which were stored at -80°C before until analysis by LC-MS/MS.

**Physicochemical Properties Experiments.** The partition coefficient (CLogP) values were calculated by ACD Lab software. The distribution coefficients (log *D*, pH 7.4) were determined by Gemini Profiler instrument (pION) based on the methods of Avdeef and Tsinman, guiding by "gold standard" Avdeef−Bucher potentiometric titration method[34]. The Permeability coefficients were detected via double-sink PAMPA on a PAMPA Explorer instrument (pION). The experimental procedures were similar as previously reported[33, 35].

**Statistics.** GraphPad Prism 6.0 software was used to calculate experimental data. Values are expressed in the form of means ± SD. The data were analyzed from at least three parallel experiments. Significant differences between two groups were indicated as $*P < 0.05$, $**P < 0.01$, $***P < 0.001$.

## ASSCIATED CONTENT

### Supporting Information

Information of supplemental tables for Hsp90 ATPase activity in vitro, the change of Gibbs free energy from computational calculation and ITC experiments, figures for

binding affinities determined by BLI and ITC assay, CPMG spectrum, calculation of the change of Gibbs free energy based on MD simulation and H&E of organs in different groups of mice (PDF)

Molecular formula strings (CSV)

## AUTHOR INFORMATION

### Corresponding Authors

*For QD.Y.: Phone/Fax: +86 025 83271351. E-mail: youqd@163.com

*For XL.X.: Phone: +86 13851822757. E-mail: xuxiao_li@126.com

### ORCID

Lei Wang: 0000-0002-8181-5644

Xiaoli Xu: 0000-0002-1126-2538

Qidong You: 0000-0002-8587-0122

### Author Contributions

The manuscript was written through contributions of all authors. All authors have given approval to the final version of the manuscript.

### Notes

The authors declare no competing financial interest.

## ACKNOWLEDGMENTS

This study was supported by projects 81573346, 81872737, 81773639 and 81930100 of the National Natural Science Foundation of China; BK20190559 of the Natural Science Foundation of Jiangsu Province of China; CPU2018GY02 of the Double First Class Innovation Team of China Pharmaceutical University; the National Science & Technology Major Project “Key New Drug Creation and Manufacturing Program”, China (No: 2018ZX09711002, 2017ZX09302003 and 2015ZX09101032); the Open Project of State Key Laboratory of Natural Medicines (SKLNMZZCX201803); China Postdoctoral Science Foundation (No: 2018M642376); the Priority Academic Program Development of Jiangsu Higher Education Institutions.

## ABBREVIATIONS

Hsp90, heat shock protein 90; Cdc37, cell division cycle 37; PPI, protein-protein interaction; HSR, heat shock response; CDK, cell cycle dependent kinase; PDB, protein data bank; CK2, casein kinase 2; ATP, adenosine 5'-triphosphate; ATPase, adenosine triphosphatase; co-IP, co-immunoprecipitation; HTRF, homogeneous time-resolved fluorescence; NMR, nuclear magnetic resonance; HSQC, heteronuclear single quantum correlation; STD, saturation transfer difference; $IC_{50}$, half-maximum inhibitory concentration; SAR, structure-activity relationship; SPR, structure-property relationship; HPLC, high-performance liquid chromatography; BLI, biolayer interferometry; ITC, isothermal titration calorimetry; WT, wild type; CPMG, Carr-Purcell-Meiboom-Gill; MD, molecular dynamics; RMSD, root mean square deviation; CETSA, cellular thermal shift assay; PK, pharmacokinetic; HE, hematoxylineosin; GR, glucocorticoid receptor; ESI, electrospray ionization; BOC, *tert*-butoxycarbonyl; LogP, logarithm of partition coefficient; cLogP, calculated logP; DCM, tert-butoxycarbonyl; DMSO, dimethyl sulfoxide; *T*, absolute temperature in units of kelvins (K)

## REFERENCES

(1) Whitesell, L.; Lindquist, S. L., HSP90 and the chaperoning of cancer. *Nat. Rev. Cancer*. **2005,** *5*, 761-772.

(2) Xia, Y.; Rocchi, P.; Iovanna, J. L.; Peng, L., Targeting heat shock response pathways to treat pancreatic cancer. *Drug Discov. Today*. **2012,** *17*, 35-43.

(3) DeZwaan, D. C.; Freeman, B. C., HSP90 manages the ends. *Trends Biochem. Sci*. **2010,** *35*, 384-391.

(4) Chiosis, G.; Dickey, C. A.; Johnson, J. L., A global view of Hsp90 functions. *Nat. Struct. Mol. Biol.* **2013,** *20*, 1-4.

(5) Neckers, L.; Workman, P., Hsp90 molecular chaperone inhibitors: are we there yet? *Clin. Cancer*

*Res.* **2012,** *18*, 64-76.

(6) Biamonte, M. A.; Van de Water, R.; Arndt, J. W.; Scannevin, R. H.; Perret, D.; Lee, W. C., Heat shock protein 90: inhibitors in clinical trials. *J. Med. Chem.* **2010,** *53*, 3-17.

(7) Wang, M.; Shen, A.; Zhang, C.; Song, Z.; Ai, J.; Liu, H.; Sun, L.; Ding, J.; Geng, M.; Zhang, A., Development of heat shock protein (Hsp90) inhibitors to combat resistance to tyrosine kinase inhibitors through Hsp90-kinase interactions. *J. Med. Chem.* **2016,** *59*, 5563-5586.

(8) Garcia-Carbonero, R.; Carnero, A.; Paz-Ares, L., Inhibition of HSP90 molecular chaperones: moving into the clinic. *The Lancet Oncology*. **2013,** *14*, e358-e369.

(9) Hong, D. S.; Banerji, U.; Tavana, B.; George, G. C.; Aaron, J.; Kurzrock, R., Targeting the molecular chaperone heat shock protein 90 (HSP90): Lessons learned and future directions. *Cancer Treat. Rev.* **2013,** *39*, 375-387.

(10) Bhat, R.; Tummalapalli, S. R.; Rotella, D. P., Progress in the discovery and development of heat shock protein 90 (Hsp90) inhibitors. *J. Med. Chem.* **2014,** *57*, 8718-8728.

(11) Trepel, J.; Mollapour, M.; Giaccone, G.; Neckers, L., Targeting the dynamic HSP90 complex in cancer. *Nat. Rev. Cancer*. **2010,** *10*, 537-549.

(12) Taipale, M.; Krykbaeva, I.; Koeva, M.; Kayatekin, C.; Westover, K. D.; Karras, G. I.; Lindquist, S., Quantitative analysis of HSP90-client interactions reveals principles of substrate recognition. *Cell*. **2012,** *150*, 987-1001.

(13) McClellan, A. J.; Xia, Y.; Deutschbauer, A. M.; Davis, R. W.; Gerstein, M.; Frydman, J., Diverse cellular functions of the Hsp90 molecular chaperone uncovered using systems approaches. *Cell*. **2007,** *131*, 121-135.

(14) Miyata, Y.; Nishida, E., CK2 controls multiple protein kinases by phosphorylating a kinase-targeting molecular chaperone, Cdc37. *Mol. Cell. Biol.* **2004,** *24*, 4065-4074.

(15) Roe, S. M.; Ali, M. M.; Meyer, P.; Vaughan, C. K.; Panaretou, B.; Piper, P. W.; Prodromou, C.; Pearl, L. H., The mechanism of Hsp90 regulation by the protein kinase-specific cochaperone p50(cdc37). *Cell*. **2004,** *116*, 87-98.

(16) Verba, K. A.; Wang, R. Y. R.; Arakawa, A.; Liu, Y. X.; Shirouzu, M.; Yokoyama, S.; Agard, D. A., Atomic structure of Hsp90-Cdc37-Cdk4 reveals that Hsp90 traps and stabilizes an unfolded kinase.

*Science*. **2016,** *352*, 1542-1547.

(17) Wang, L.; Li, L.; Gu, K.; Xu, X. L.; Sun, Y.; You, Q. D., Targeting Hsp90-Cdc37: a promising therapeutic strategy by inhibiting Hsp90 chaperone function. *Curr. Drug Targets*. **2017,** *18*, 1572-1585.

(18) Gray, P. J., Jr.; Prince, T.; Cheng, J.; Stevenson, M. A.; Calderwood, S. K., Targeting the oncogene and kinome chaperone CDC37. *Nat. Rev. Cancer*. **2008,** *8*, 491-495.

(19) Bachman, A. B.; Keramisanou, D.; Xu, W.; Beebe, K.; Moses, M. A.; Vasantha Kumar, M. V.; Gray, G.; Noor, R. E.; van der Vaart, A.; Neckers, L.; Gelis, I., Phosphorylation induced cochaperone unfolding promotes kinase recruitment and client class-specific Hsp90 phosphorylation. *Nat Commun*. **2018,** *9*, 265.

(20) Ihama, F.; Yamamoto, M.; Kojima, C.; Fujiwara, T.; Matsuzaki, K.; Miyata, Y.; Hoshino, M., Structural characterization of the N-terminal kinase-interacting domain of an Hsp90-cochaperone Cdc37 by CD and solution NMR spectroscopy. *Biochim Biophys Acta Proteins Proteom*. **2019,** *1867*, 813-820.

(21) Stetz, G.; Verkhivker, G. M., Functional role and hierarchy of the intermolecular interactions in binding of protein kinase clients to the Hsp90-Cdc37 chaperone: structure-based network modeling of allosteric regulation. *J. Chem. Inf. Model.* **2018,** *58*, 405-421.

(22) Penkler, D. L.; Atilgan, C.; Tastan Bishop, O., Allosteric modulation of human Hsp90alpha conformational dynamics. *J. Chem. Inf. Model.* **2018,** *58*, 383-404.

(23) Zhang, T.; Hamza, A.; Cao, X.; Wang, B.; Yu, S.; Zhan, C. G.; Sun, D., A novel Hsp90 inhibitor to disrupt Hsp90/Cdc37 complex against pancreatic cancer cells. *Mol. Cancer Ther.* **2008,** *7*, 162-170.

(24) Boridy, S.; Le, P. U.; Petrecca, K.; Maysinger, D., Celastrol targets proteostasis and acts synergistically with a heat-shock protein 90 inhibitor to kill human glioblastoma cells. *Cell Death Dis.* **2014,** *5*, e1216.

(25) Zhang, T.; Li, Y.; Yu, Y.; Zou, P.; Jiang, Y.; Sun, D., Characterization of celastrol to inhibit hsp90 and cdc37 interaction. *J. Biol. Chem.* **2009,** *284*, 35381-35389.

(26) Sreeramulu, S.; Gande, S. L.; Gobel, M.; Schwalbe, H., Molecular mechanism of inhibition of the human protein complex Hsp90-Cdc37, a kinome chaperone-cochaperone, by triterpene celastrol. *Angew. Chem. Int. Ed. Engl.* **2009,** *48*, 5853-5855.

(27) Grover, A.; Shandilya, A.; Agrawal, V.; Pratik, P.; Bhasme, D.; Bisaria, V. S.; Sundar, D., Hsp90/Cdc37 chaperone/co-chaperone complex, a novel junction anticancer target elucidated by the mode of action of herbal drug Withaferin A. *BMC Bioinformatics*. **2011,** *12 Suppl 1*, S30.

(28) Huang, W.; Ye, M.; Zhang, L. R.; Wu, Q. D.; Zhang, M.; Xu, J. H.; Zheng, W., FW-04-806 inhibits proliferation and induces apoptosis in human breast cancer cells by binding to N-terminus of Hsp90 and disrupting Hsp90-Cdc37 complex formation. *Mol. Cancer*. **2014,** *13*, 150.

(29) Li, D.; Li, C.; Li, L.; Chen, S.; Wang, L.; Li, Q.; Wang, X.; Lei, X.; Shen, Z., Natural product kongensin A is a non-canonical Hsp90 inhibitor that blocks RIP3-dependent necroptosis. *Cell Chem Biol*. **2016,** *23*, 257-266.

(30) Wang, L.; Li, L.; Zhou, Z. H.; Jiang, Z. Y.; You, Q. D.; Xu, X. L., Structure-based virtual screening and optimization of modulators targeting Hsp90-Cdc37 interaction. *Eur. J. Med. Chem.* **2017,** *136*, 63-73.

(31) Chen, X.; Liu, P.; Wang, Q.; Li, Y.; Fu, L.; Fu, H.; Zhu, J.; Chen, Z.; Zhu, W.; Xie, C.; Lou, L., DCZ3112, a novel Hsp90 inhibitor, exerts potent antitumor activity against HER2-positive breast cancer through disruption of Hsp90-Cdc37 interaction. *Cancer Lett.* **2018,** *434*, 70-80.

(32) Wang, L.; Zhang, L.; Li, L.; Jiang, J.; Zheng, Z.; Shang, J.; Wang, C.; Chen, W.; Bao, Q.; Xu, X.; Jiang, Z.; Zhang, J.; You, Q., Small-molecule inhibitor targeting the Hsp90-Cdc37 protein-protein interaction in colorectal cancer. *Science Advances*. **2019**, eaax2277.

(33) Jiang, Z. Y.; Xu, L. L.; Lu, M. C.; Chen, Z. Y.; Yuan, Z. W.; Xu, X. L.; Guo, X. K.; Zhang, X. J.; Sun, H. P.; You, Q. D., Structure-activity and structure-property relationship and exploratory in vivo evaluation of the nanomolar Keap1-Nrf2 protein-protein interaction inhibitor. *J. Med. Chem.* **2015,** *58*, 6410-6421.

(34) Avdeef, A.; Tsinman, O., Miniaturized rotating disk intrinsic dissolution rate measurement: effects of buffer capacity in comparisons to traditional wood's apparatus. *Pharm. Res.* **2008,** *25*, 2613-2627.

(35) Jiang, F.; Wang, H. J.; Jin, Y. H.; Zhang, Q.; Wang, Z. H.; Jia, J. M.; Liu, F.; Wang, L.; Bao, Q. C.; Li, D. D.; You, Q. D.; Xu, X. L., Novel tetrahydropyrido[4,3-d]pyrimidines as potent inhibitors of chaperone heat shock protein 90. *J. Med. Chem.* **2016,** *59*, 10498-10519.

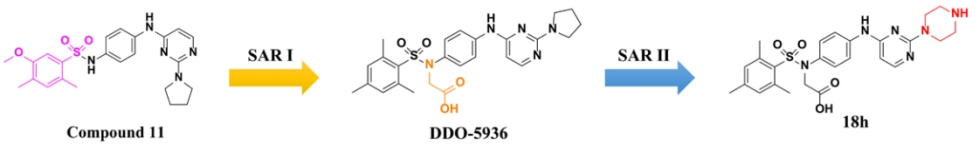


Compound 11

HTRF: IR = 56.3 % (@100 μM)
BLI : $K_D$ = 21.10 μM
ITC: undetectable
NMR : undetectable
ATPase : ≈ 30% (@100 μM)

DDO-5936

HTRF: IR = 72.6 % (@100 μM)
BLI : $K_D$ = 7.41 μM
ITC : $K_d$ = 5.68 μM
NMR : detectable
ATPase: $IC_{50}$ > 50 μM
$IC_{50}$ (HCT116)= 10.24 μM
Stability: ×
Oral administration: ×

18h

HTRF: IR = 99.8% (@100 μM)
BLI : $K_D$ = 0.50 μM
ITC : $K_d$ = 0.63 μM
NMR : detectable
ATPase: $IC_{50}$ > 50 μM
$IC_{50}$ (HCT116)= 1.73μM
Stability: √
Oral administration: √